UNITED NATIONS EDUCATIONAL, SCIENTIFIC AND CULTURAL ORGANIZATION
INTERNATIONAL ATOMIC ENERGY AGENCY
INTERNATIONAL CENTRE FOR THEORETICAL PHYSICS
I.C.T.P., P.O. BOX 586, 34100 TRIESTE, ITALY, CABLE: CENTRATOM TRIESTE

H4.SMR/984-16

Winter College on Quantum Optics: Novel Radiation Sources

3-21 March 1997

Synchrotron radiation and lasers in atomic and molecular physics

M. Aslam Baig

Atomic and Molecular Physics Lab, Quaid-i-Azam University,
Islamabad, Pakistan

Synchrotron Radiation

- Energy loss

$$\Delta E = \frac{88.5}{R} E^4 \quad (KeV)$$

- Radiated Power

$$P = 88.5\, E^4\, I/R \quad (K.W)$$

- Radiated Power by each relativistic electron

$$P = \frac{2}{3} \frac{e^2 c}{R^2} \left(\frac{E}{m_0 c^2}\right)^4 \left(\frac{1}{4\pi\varepsilon_0}\right) \quad (W)$$

- Critical wavelength

$$\lambda_c = \frac{19}{(B E^2)}$$

- Photon flux

$$N(\lambda) = 2.5 \times 10^{14}\, E\, G\left(\frac{\lambda}{\lambda_c}\right) I$$

$\lambda_c = 3.9\,\text{Å}$; $E = 2\,GeV$; $I = 300\,mA$

$\approx 3 \times 10^{13}$ photon s^{-1} mrad^{-2} $\sim 1\%$ Lund Fac.

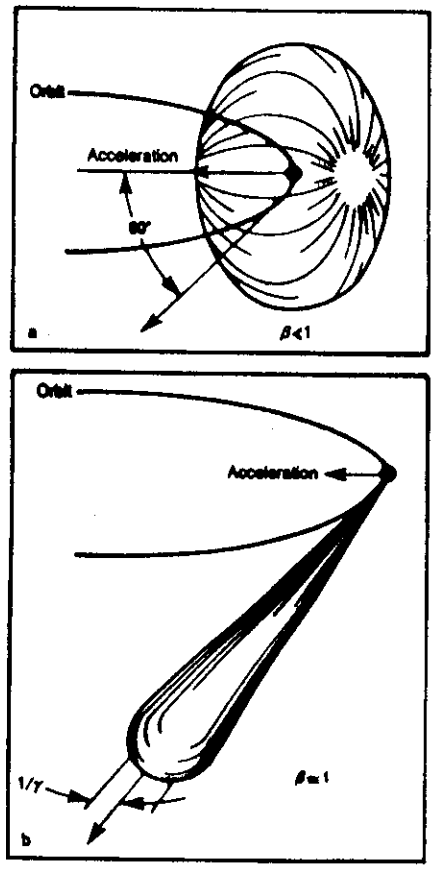

Radiation pattern of electrons in a circular orbit. The upper diagram shows the pattern for nonrelativistic electrons predicted by Joseph Larmor. The lower diagram shows the pattern for highly relativistic electrons: the radiation is concentrated in a narrow cone; the spectrum also extends to very high frequencies.


1 eV
100 eV
1 keV
10 keV
100 keV
Energy

TABELLA I

Laboratori di ricerca con luce di sincrotrone

Anelli di accumulazione (1)	Energia (GeV)	Corrente (mA)	Raggio di curvatura (m)	Energia critica (2) (KeV)
DORIS, Hamburg, Germania	1.5-4.0	250	12.2	11.6
SPEAR, Stanford, USA	1.5-4.0	5-35	12.7	11.1
VEPP-3, Novosibirsk, URSS	2.25	200	6.0	4.2
VEPP-2M, Novosibirsk, URSS	67	100	1.22	54
ACO, Orsay, Francia (DLS)	54	100	1.1	32
INS-SOR, Tokyo, Giappone (DLS)	30	100	1.0	059
TANTALUS I, Wisconsin, USA (DLS)	24	100	64	048
SURF II, NBS, Washington DC, USA (DLS)	24	50	84	036
DCI, Orsay, Francia	1.8	500	3.8	3.4
PACHRA, Moscow, URSS	1.3	10-300	4.0	1.1
IPP, Moscow, URSS (DLS) (3)	1.35	100	2.5	2.2
Daresbury, Gran Bretagna (DLS) (4)	2.0	500-1000	5.55	3.2
Brookhaven, USA (DLS) (3)	2.0	500-1000	8.1	2.2
Wisconsin, USA (DLS) (3)	2-2.5	500-1000		
Photon Factory, Giappone (DLS) (3)	2,5			
ADONE, Frascati, Italia (5)	1.5	60	5.0	1.5
Amsterdam, Olanda (DLS) (3)	1-2			
ALADDIN, Wisconsin, USA (DLS) (3)	75	500	2.0	46
Sincrotroni				
Cornell, USA	12	2	100	38
DESY, Hamburg, Germania	7.5	10-30	31.7	29.5
ARUS, Yerevan, URSS	6.0	20	24.6	19.5
NINA, Daresbury, Gran Bretagna (6)	5.0	40	20.8	13.3
BONN I, Germania	2.5	30	7.6	4.6
INS-SOR, Tokyo, Giappone	1.3	30	4.0	1.22
Frascati, Italia	1.1	10	3.6	82
C-60, Moscow, URSS	68	10	1.6	44
BONN II, Germania	5	30	1.7	16

Note

(1) Le macchine destinate unicamente a ricerche con luce di sincrotrone sono indicate con DLS.
(2) In genere si possono fare esperienze fino ad energie dell'ordine di 4-5 volte l'energia critica.
(3) In fase di progettazione.
(4) In fase di costruzione.
(5) Laboratorio in costruzione.
(6) Chiuderà nel 1977.

EXPERIMENTAL SET UP

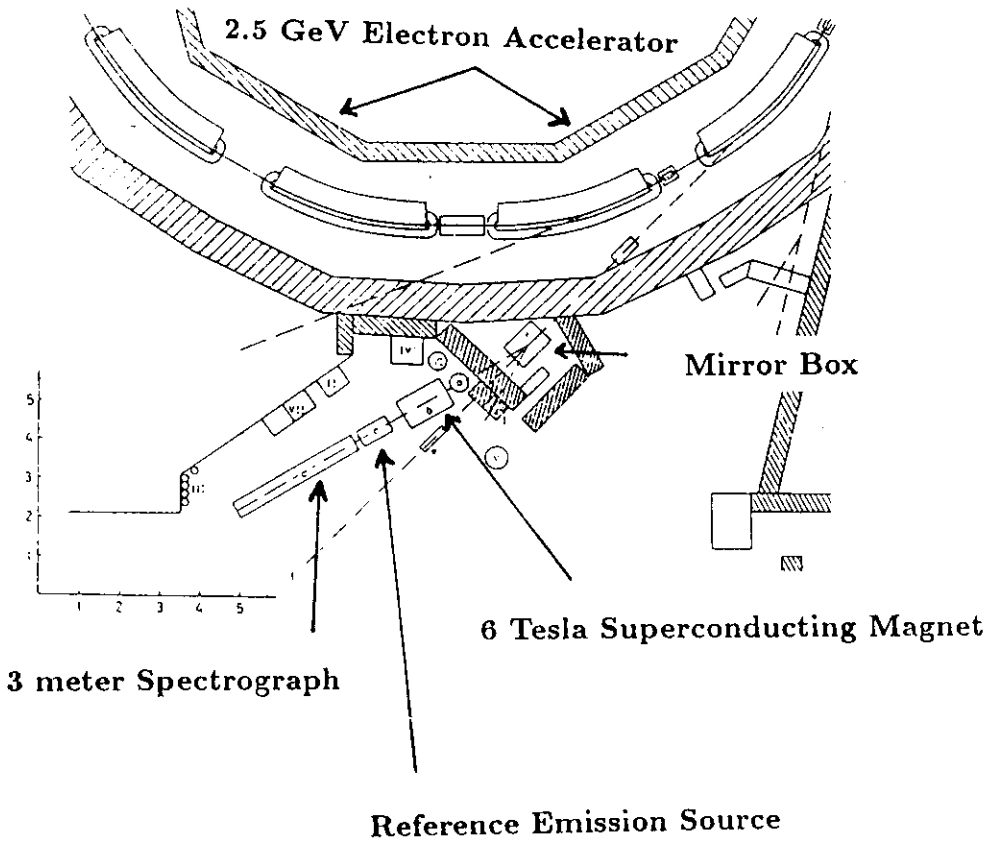

ABSORPTION STUDIES:

- Precise Energy Level Measurements
- Photoionization Cross Section
- Many- Body Effects / Double Excitation
- Configuration Interaction

ZEEMAN SPECTROSCOPIC STUDIES:

- Total Angular Momentum Assignments
- Wavefunction Mixing Determinations
- g - values
- Inter n,l- Mixing
- Quasi Landau Resonances

MAGNETO - OPTICAL STUDIES:

- Oscillator Strengths Measurements
- Relative f-values Measurements

PRACTICAL APPLICATIONS:

- Chemical abundances determinations:

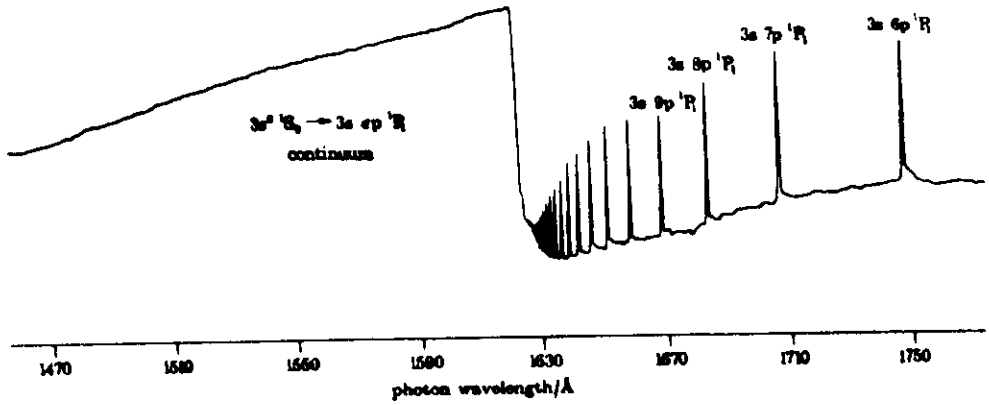

FIGURE 3. The principal series due to excitation of $3s^2\ ^1S_0 \longrightarrow 3s\,np\ ^1P_1$ in Mg I, showing the sudden onset and uniform decrease of continuous absorption above the first ionization threshold. The apparently discontinuous rise at threshold is an artefact, as traces at higher magnification reveal. The decrease in continuous absorption with decreasing wavelength persists until the structures of figure 2 are reached.

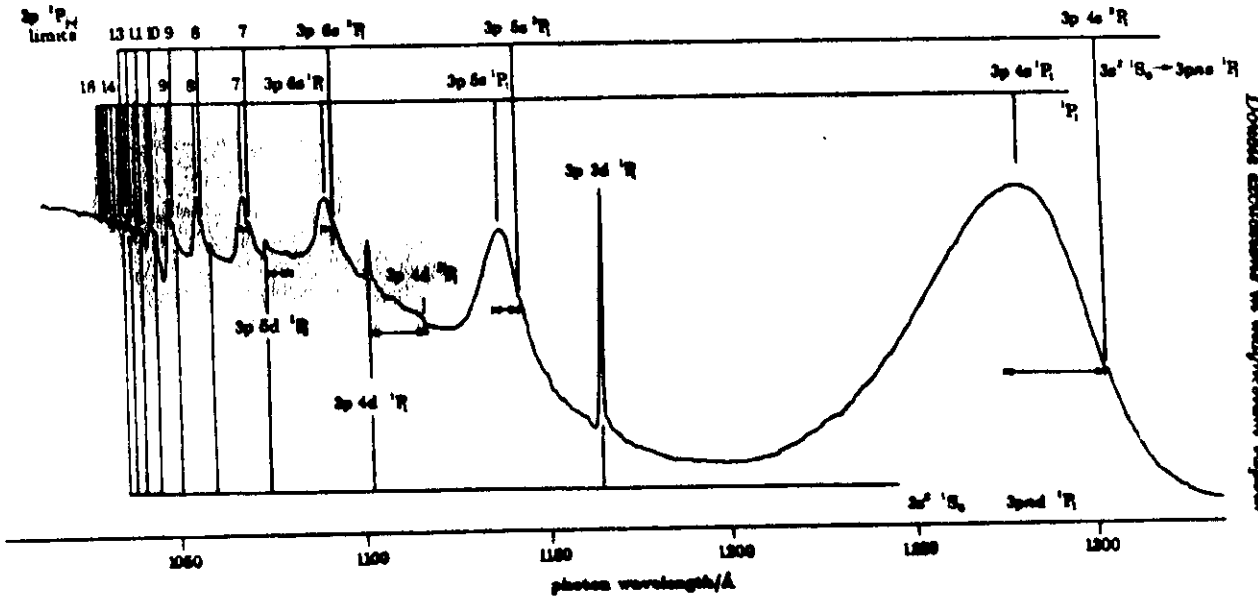

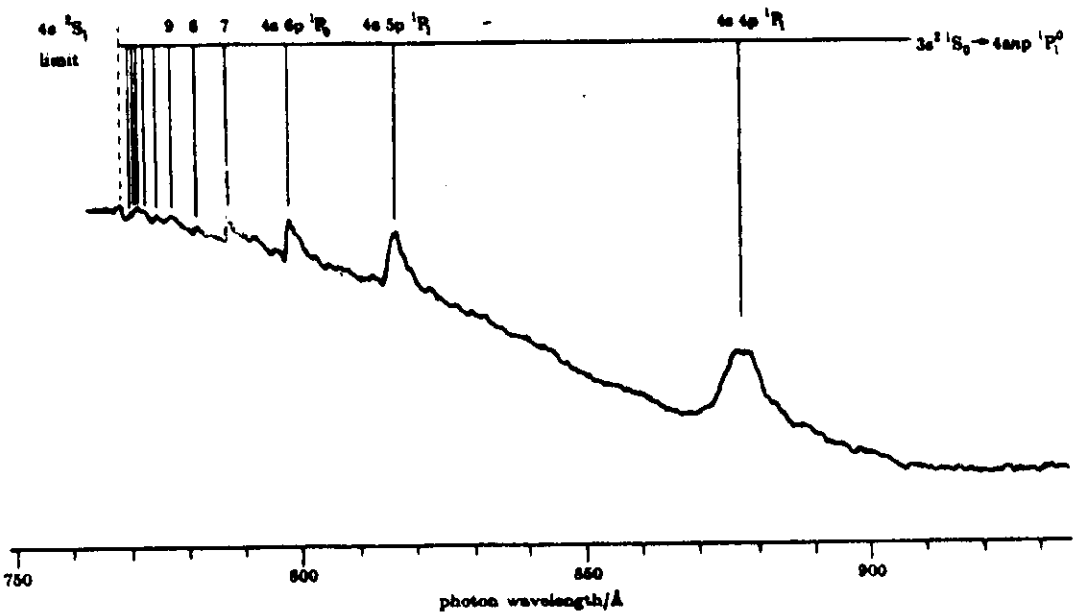

FIGURE 4. Showing the series due to double excitation $3s^2\ ^1S_0 \longrightarrow 4s\,np\ ^1P_1^0$ of Mg I.

Absorption Spectrum of Helium
"Doubly excited States"

Photograph

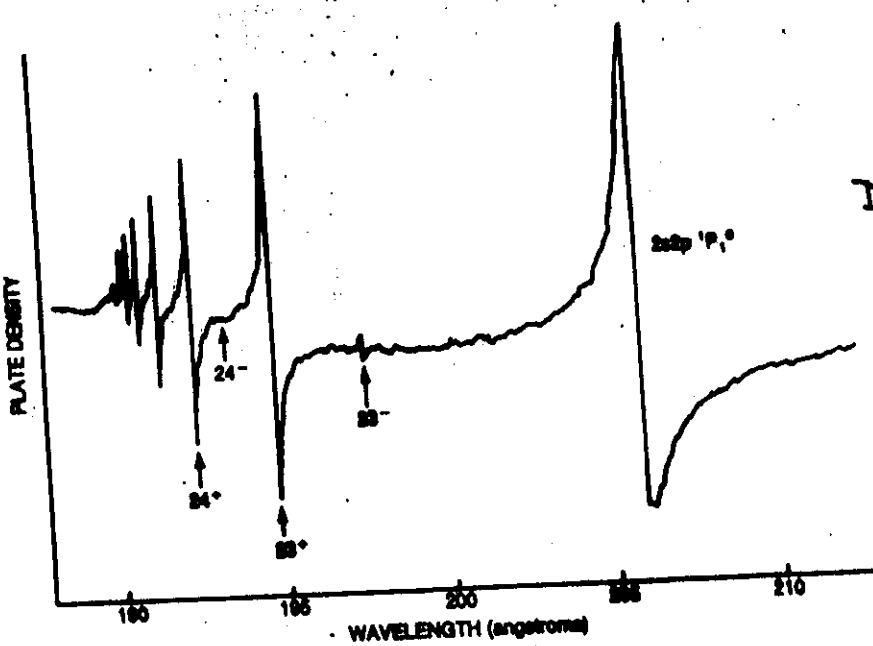

Densitometeric Trace

Isolated Autoionizing Resonance

The absorption line profiles in the ionization continuum of atomic spectra are represented as: (Fano, 1961)

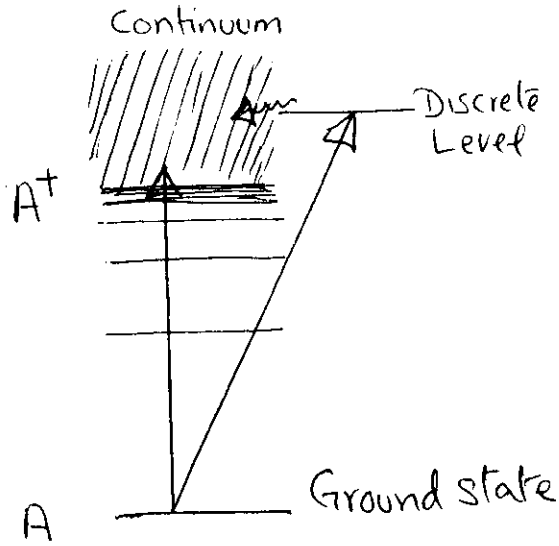

$$\sigma(\epsilon) = \sigma_a \left[\frac{(q+\epsilon)^2}{1+\epsilon^2} \right] + \sigma_b$$

Here $\epsilon = \dfrac{(E - E_R)}{\frac{1}{2}\Gamma}$

q = line profile index.

σ_a = part of the continuum which interacts with the discrete level

σ_b = part of the continuum which doesnot interact with the discrete level.

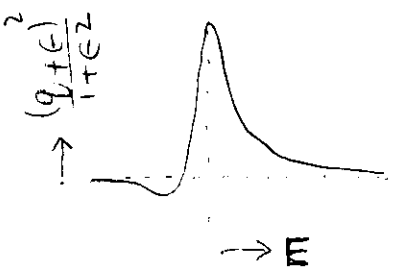

Double Excitation in Helium

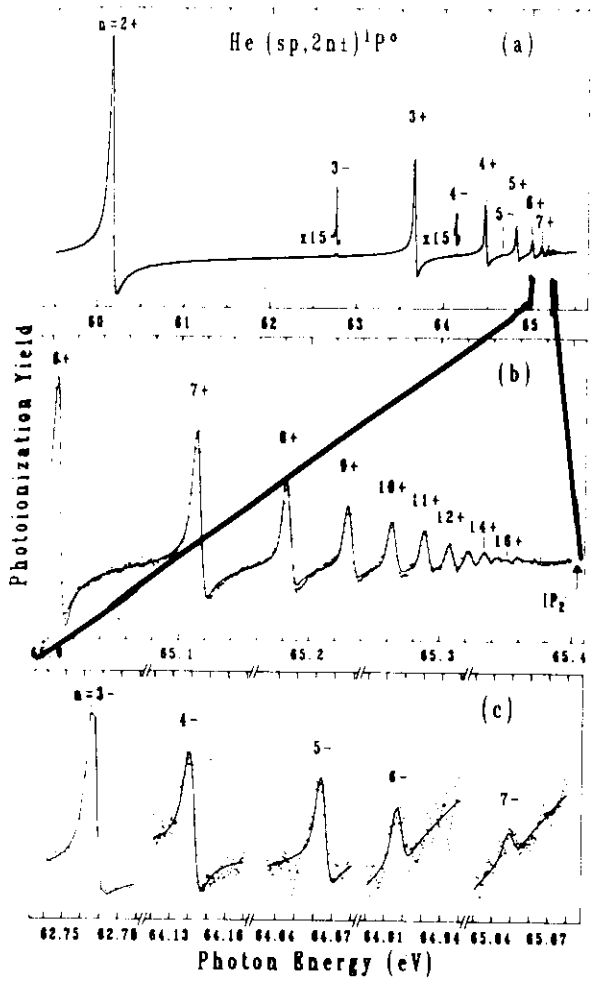

FIG. 1. Autoionizing states of double-excited He below the $N=2$ threshold (IP_2) of He: (a) overview, (b) magnification of the $n \geq 6$ region, and (c) "$2n-$" states.

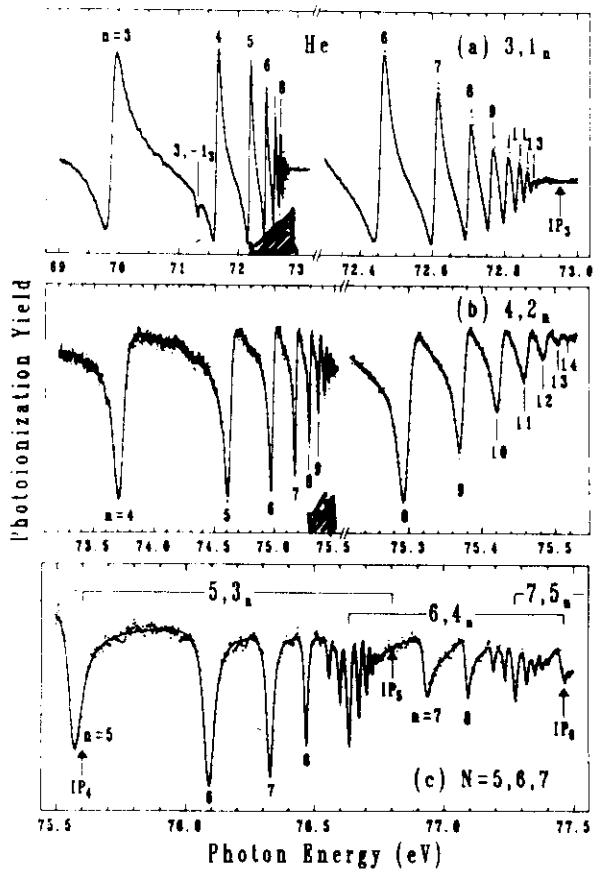

FIG. 2. Autoionizing states of He: (a) below the $N=3$ threshold (IP_3), (b) below the $N=4$ threshold (IP_4), and (c) below the $N=5$ and 6 thresholds (IP_5, IP_6). The high-n regions are shown magnified on the right-hand sides in (a) and (b). Note the overlapping of series in (c).

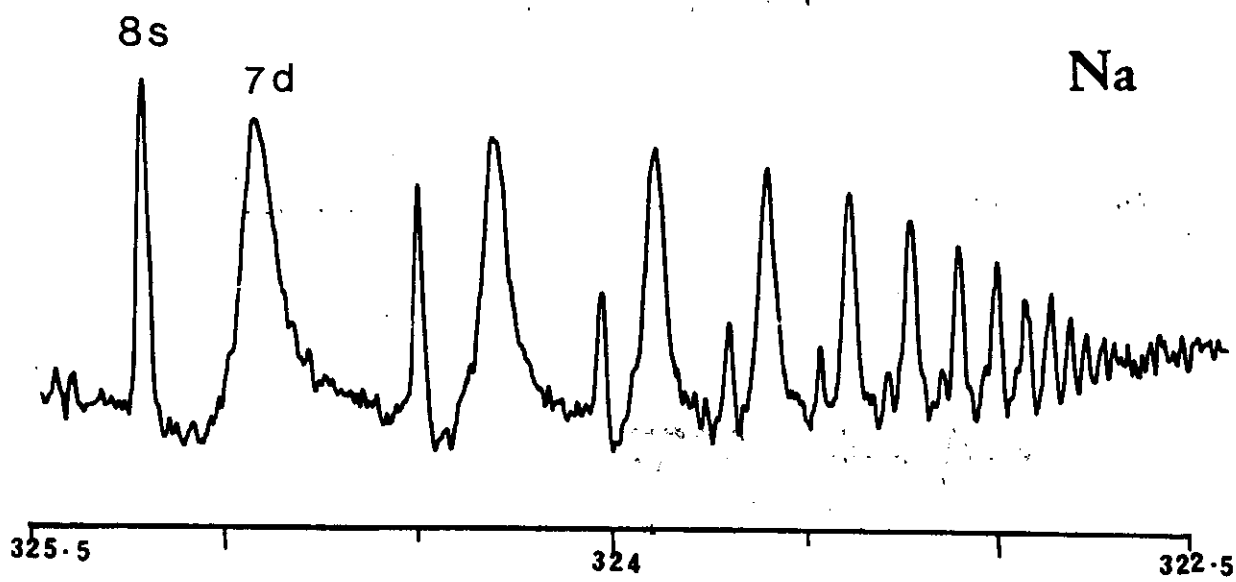
8s
7d
Na
325·5
324
322·5

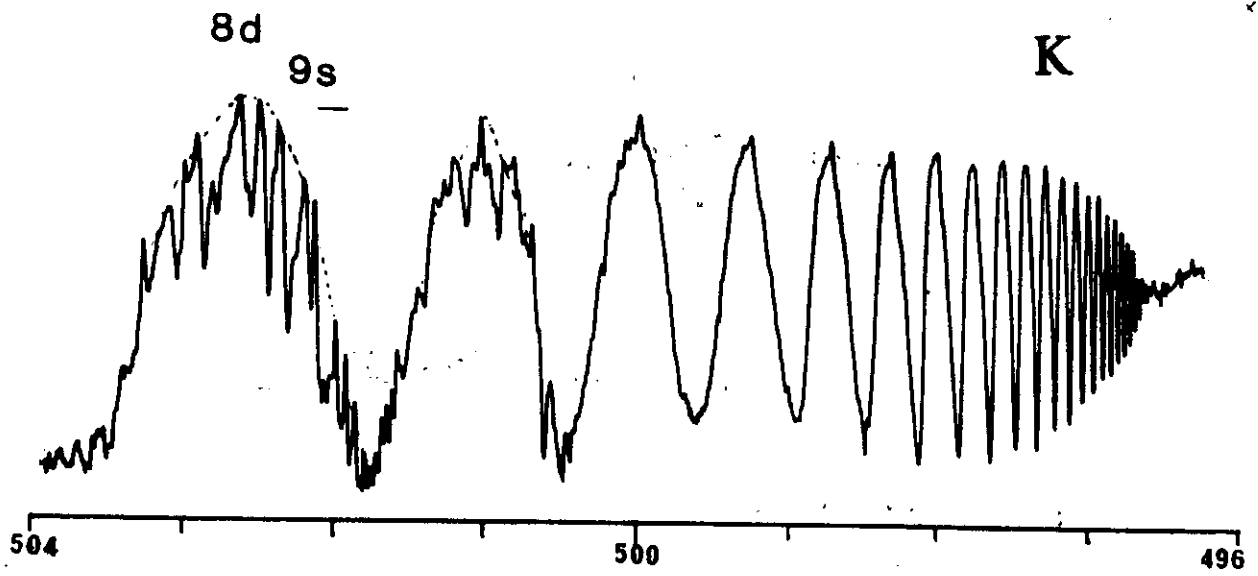
8d
9s
K
504
500
496

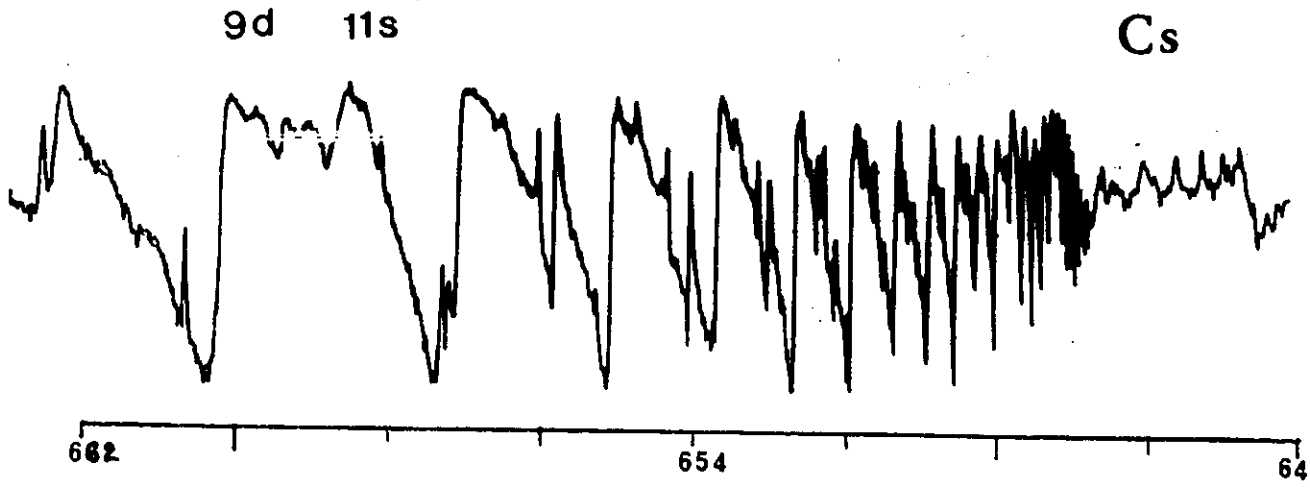
9d
11s
Cs
662
654
646

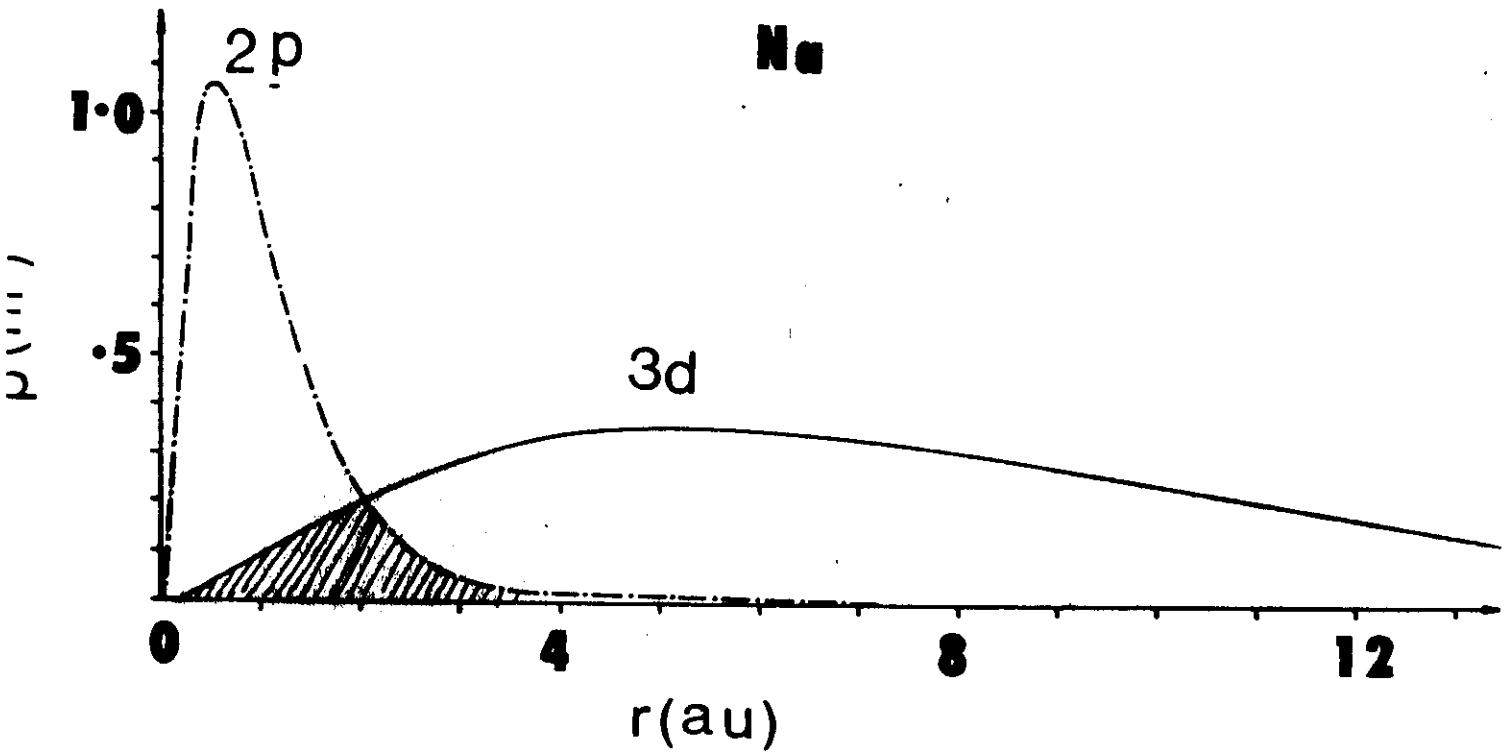

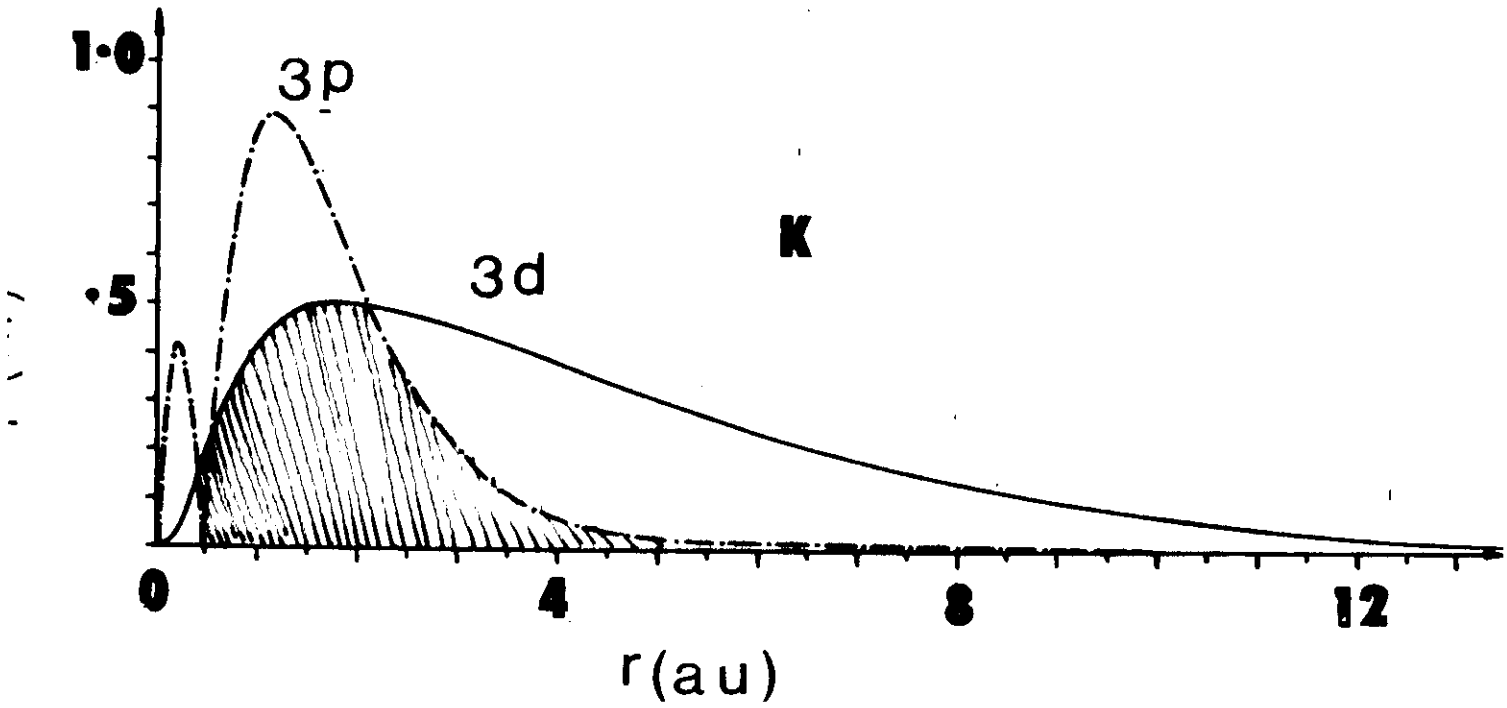

Single [illegible] SCF [illegible] calculations.

Effective Bond Numbers:

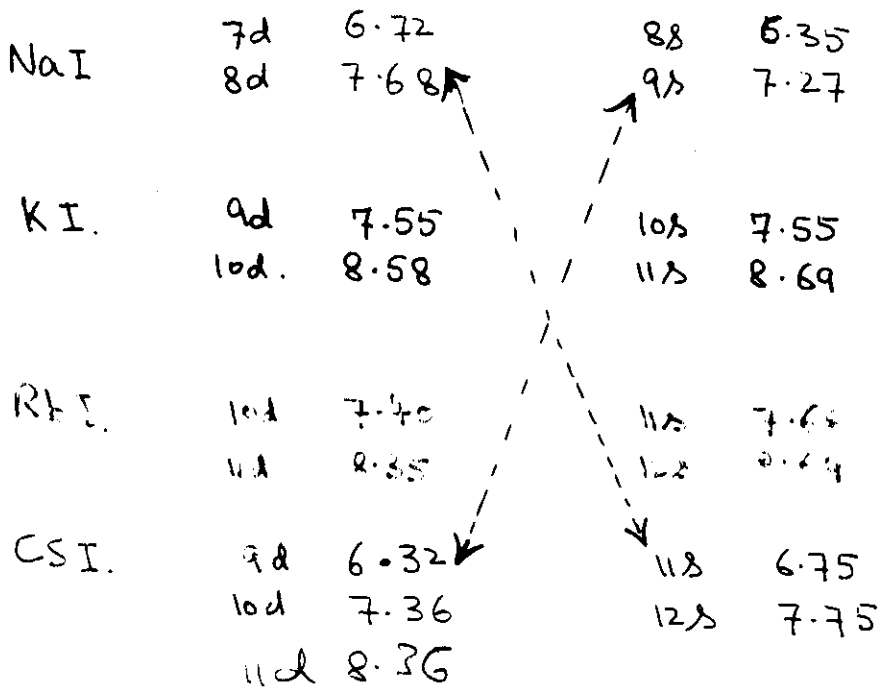

QUASI-ATOMIC RYDBERG STATES

CH_3I

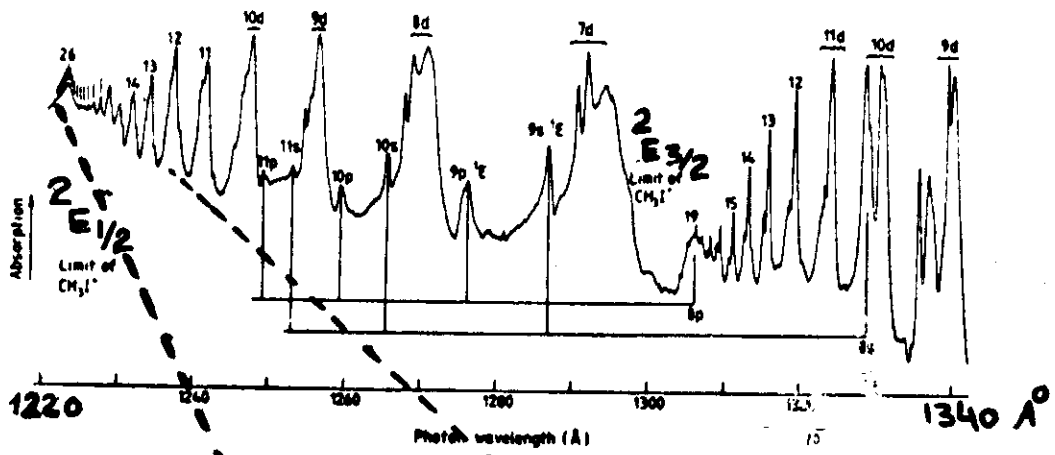

$(a\sigma)^2(e\pi)^4\ {}^1A_1 \longrightarrow (e\pi)^3({}^2E_{3/2})\ n\ell\lambda$

$\longrightarrow\ ({}^2E_{1/2})\ n\ell\lambda$

Spin Orbit Splitting = 5050 cm^{-1}.

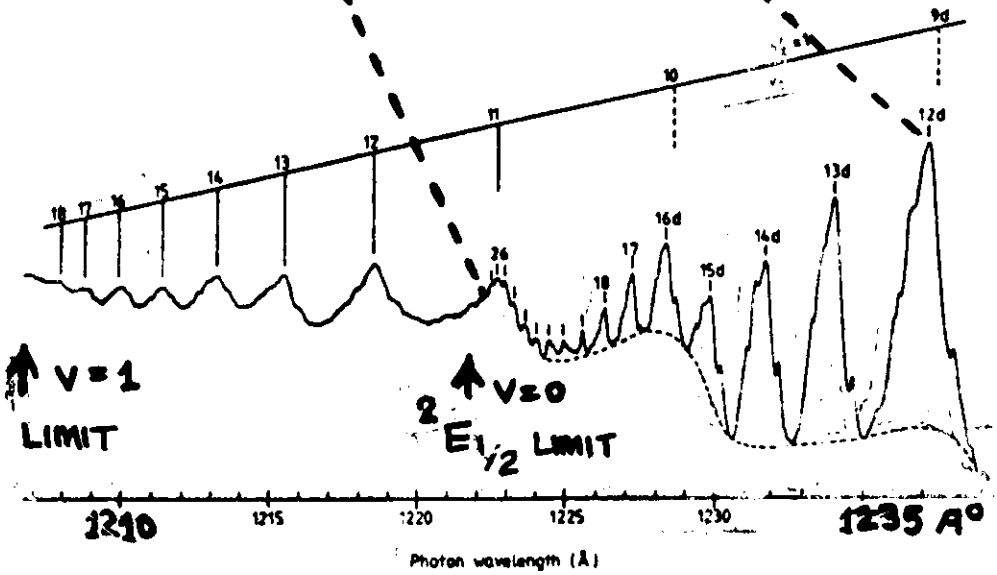

$5p^6\ {}^1S_0 \longrightarrow 5p^5({}^2P_{3/2})$ ns $[3/2]^\circ_1$

nd $[1/2]^\circ_1$

nd $[3/2]^\circ_1$

$\longrightarrow\ ({}^2P_{1/2})$ ns $[1/2]^\circ_1$

nd $[3/2]^\circ_1$

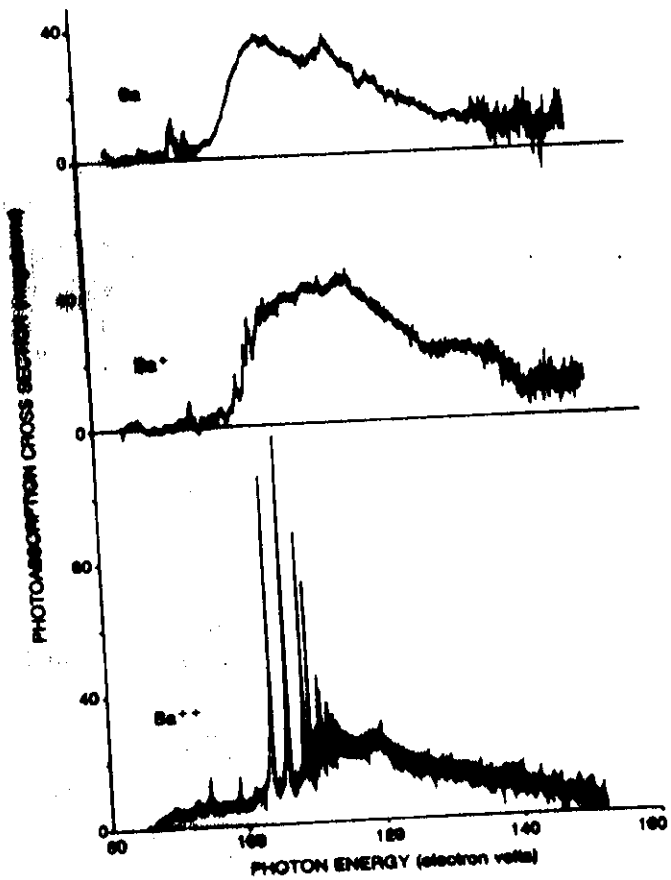
40
0
Ba
Ba+
0
80
40
Ba++
0
80
100
120
140
160
PHOTON ENERGY (electron volts)

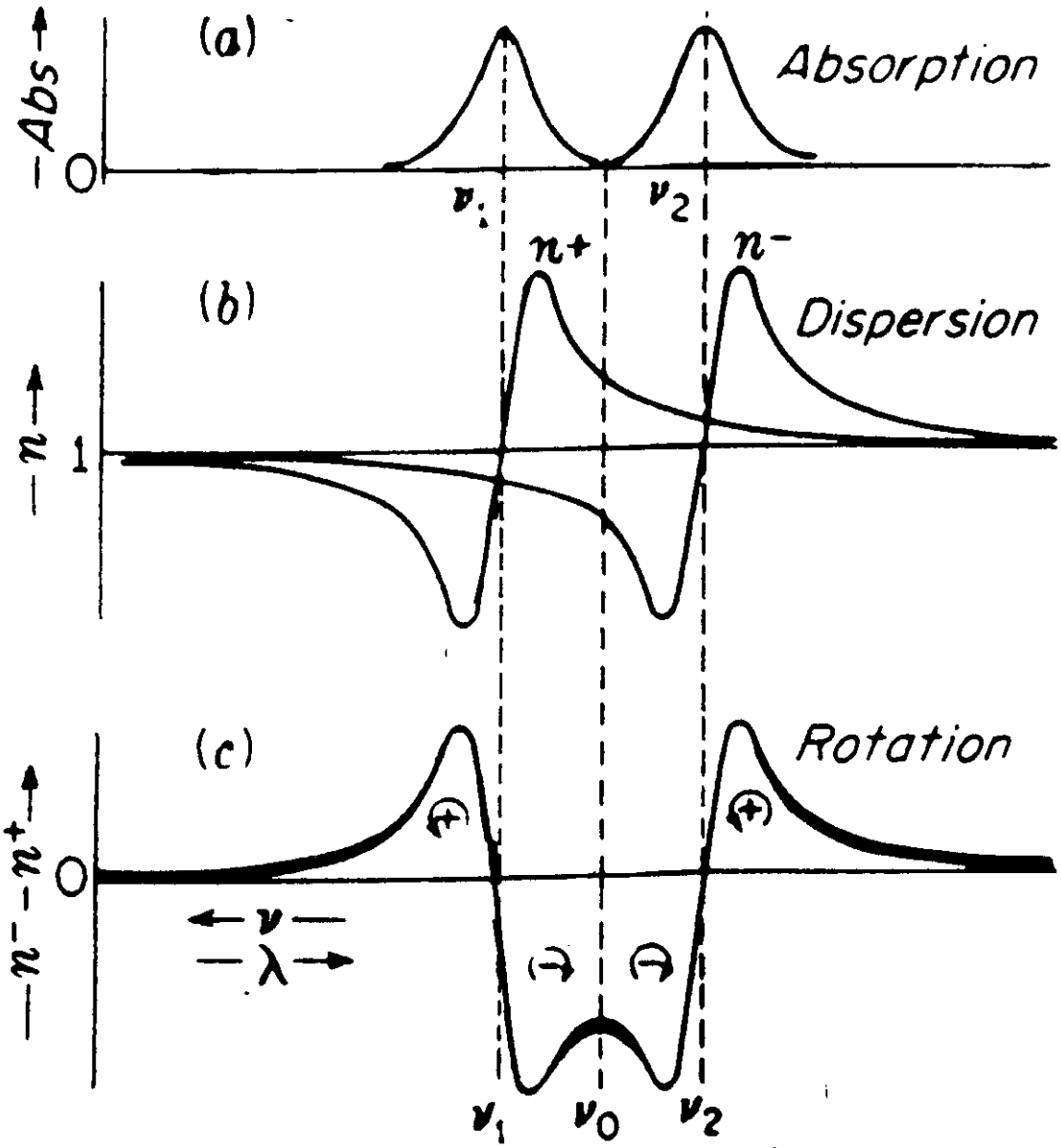

Zeeman splitting: $\Delta\omega_{zee} = \frac{e}{2m} B_g$

Diamagnetic Zeeman effect: $\Delta\omega_{dzee} = \frac{e^2 a_0^2}{mh} \cdot \frac{B^2}{Z^2}(n^4 - n^2)$

FARADAY ROTATION

$$E_{\pm} = E_0 (\mathbf{i} \pm i\mathbf{j}) \exp[i\omega(t - \hat{n}_{\pm} z/c)] \quad \text{....(1)}$$

$\mathbf{i}, \mathbf{j}, \mathbf{k}$ are unit vectors

$\hat{n}_{\pm}$ is the complex refractive index.

$$\hat{n}_{\pm} = n_{\pm} - ik_{\pm}$$

$$E = E_+ + E_- = E_x \mathbf{i} + E_y \mathbf{j} \quad \text{....(2)}$$

where $\bar{z} = z\omega/c$

$$\hat{\Phi} = \underbrace{\phi - i\theta}_{\text{Two different contributions.}}$$

$$\phi = \tfrac{1}{2}(n_+ - n_-)\bar{z} \quad \text{(Faraday Rotation)}$$

$$\theta = \tfrac{1}{2}(k_+ - k_-)\bar{z} \quad \text{(circular birefringence)}$$

The incident intensity I_0 is related to E_0 by letting $z = 0$ thus:

$$I_0 = 4E_0^2 \quad \text{..... (4)}$$

$$E_y E_y^* = E_0^2 \{[\exp(-k_+\bar{z}) - \exp(-k_-\bar{z})]^2 + 4\exp[-(k_+ - k_-)\bar{z}] \cdot \sin^2(n_+ - n_-)\bar{z}/2\}$$

Let $a_{\pm} = 2\omega k_{\pm}/c$

$a_{\pm}$ / intensity absorption coefficient

To use this relation for practical calculation, we express a_+, a_-, n_+ & n_- as follows:

$$a_{\pm} = \frac{e^2 N f}{mc} \frac{\Gamma/4\pi}{(\nu_0 - \nu \pm \alpha)^2 + (\Gamma/4\pi)^2}$$

$$n_{\pm} = \frac{e^2 N f}{4\pi m} \frac{1}{(\nu_0 \pm \alpha)} \cdot \frac{\nu_0 - \nu \pm \alpha}{(\nu_0 - \nu \pm \alpha)^2 + (\Gamma/4\pi)^2} \quad \ldots (6)$$

where $\alpha = \frac{e}{4\pi mc} B$

Substituting eqn(6) into Eq(5) allows us to calculate the magneto-optical rotation for Faraday crossed polariser & analyser.

$$\phi = -\frac{N f l B e^3}{8\pi m^2 c^2} \cdot \frac{(2\nu_0\nu - \nu^2)[(\nu_0 - \nu)^2 - \alpha^2] - \nu^2 (\Gamma/4\pi)^2}{(\nu_0^2 - \alpha^2)[(\nu_0 - \nu + \alpha)^2 + (\Gamma/4\pi)^2][(\nu_0 - \nu - \alpha)^2 + (\Gamma/4\pi)^2]} \quad -(7)$$

As the frequency of the light is varied, starting from the far wing of a line and moving in towards the zero field line centre, the rotation angle grows from zero to high values, and crossed polarisers transmit a series of "beats" which correspond to maxima and minima in the function $\sin^2\phi$.

Neglecting all effects due to absorption, to treat them as maxima and minima in the function $\sin^2\phi$, and assuming [illegible], then eq(7) reduces to the far wing Formula (Mitchell & Zemansky)

$$\phi = \frac{N f l B e^3}{8\pi m^2 c^2} \cdot \frac{1}{(\nu - \nu_0)^2} \quad ---(8)$$

Rydberg States of MgI.

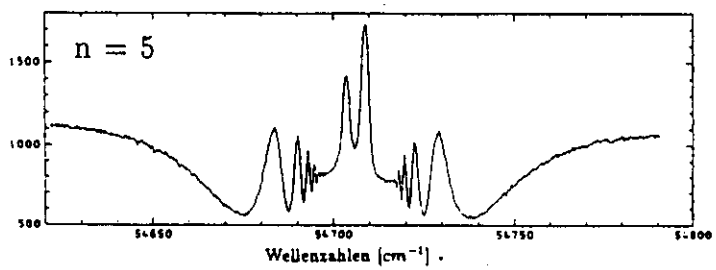

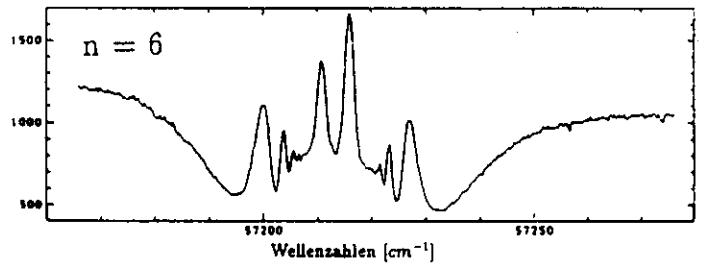

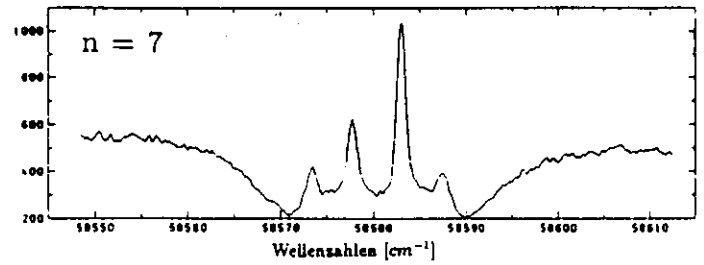

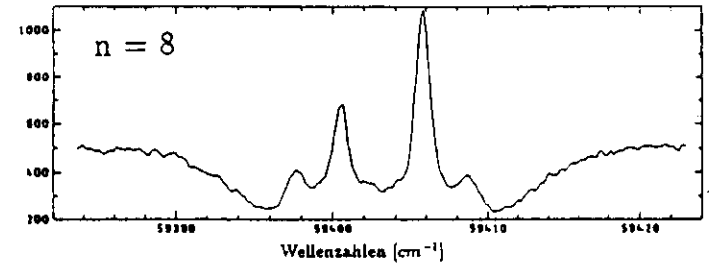

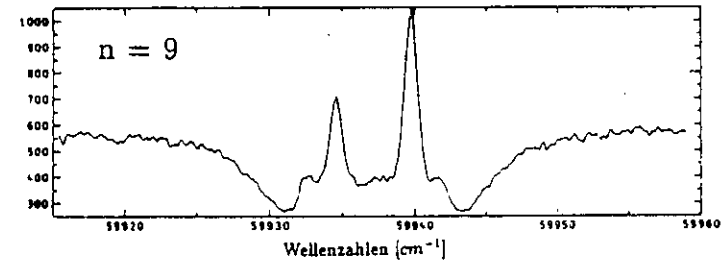

oscillator Strengths of SrI Principal series

n	λ_0 (Å)	n^*	f (present)	f (PS)†	f(PRT)‡
11	2253.954	8.372	0.008 51§	0.008 91 ± 15%	0.008 51 ± 12%
12	2238.350	9.346	0.005 31 ± 0.6%	0.005 25 ± 15%	0.005 13 ± 12%
13	2226.997	10.330	0.003 51 ± 0.7%	0.003 72 ± 15%	0.003 63 ± 12%
14	2218.507	11.319	0.002 58 ± 0.8%	0.002 57 ± 15%	0.002 57 ± 12%
15	2211.999	12.311	0.001 87 ± 1.3%	0.002 09 ± 15%	0.001 86 ± 12%
16	2206.927	13.302	0.001 41 ± 1.5%	0.001 48 ± 15%	0.001 45 ± 15%
17	2202.863	14.302	0.001 10 ± 1.7%	—	0.001 07 ± 15%
18	2199.579	15.301	0.009 24 ± 1.8%	—	0.000 98 ± 15%
19	2196.900	16.294	0.000 696 ± 1.9%	—	0.000 78 ± 15%
20	2194.663	17.292	0.000 555 ± 2.0%	—	0.000 66 ± 15%
21	2192.788	18.290	0.000 447 ± 2.2%	—	0.000 58 ± 15%
22	2191.196	19.293	0.000 378 ± 2.6%	—	0.000 50 ± 20%
23	2189.841	20.288	0.000 309 ± 3.2%	—	0.000 42 ± 20%
24	2188.673	21.286	0.000 268 ± 3.6%	—	0.000 33 ± 20%
25	2187.652	22.288	0.000 218 ± 3.7%	—	0.000 31 ± 20%
26	2186.776	23.273	0.000 179 ± 5.6%	—	0.000 26 ± 20%
27	2186.046	24.281	0.000 149 ± 6.7%	—	—
28	2185.389	25.273	0.000 119 ± 8.3%	—	—

† PS denotes Penkin and Shabanova (1962).
‡ PRT denotes Parkinson, Reeves and Tomkins (1976).
§ All the present values are normalised onto the $n = 11$ f value given by PRT which is regarded as exact when specifying the error bars in the column of present measurements.

MgI $3snP\ ^1P_1$ series

n	n^*	ΔE	Nfl $[10^{14} cm^{-2}]$	ΔNfl[%]	$f \cdot 10^4$	$\frac{f \cdot n^{*3}}{2R} \cdot (eV)$	$f^{-1/3}$
5	3.9694	−0.863	86.401	0.4	556.1	1278.7±5.1	2.62±0.02
6	4.9624	−0.552	28.44	0.8	183.1	822.6±6.6	3.79±0.03
7	5.9584	−0.383	6.385	2	41.10	319.3±9.6	6.24±0.04
8	6.9561	−0.281	3.900	2	25.10	310.6±9.3	7.36±0.05
9	7.9546	−0.215	2.535	3	16.32	302.0±9.0	8.49±0.1
10	8.9533	−0.170	1.505	3	9.69	255.7±7.7	10.1±0.1
11	9.9527	−0.137	1.197	5	7.71	279.5±14.0	10.9±0.2
12	10.9516	−0.113	0.761	5	4.90	236.6±11.8	12.7±0.2
13	11.9513	−0.095	0.682	8	4.39	275.5±22.0	13.2±0.4
14	12.9507	−0.081	0.525	8	3.38	269.9±21.6	14.4±0.4
15	13.9507	−0.070	0.493	10	3.17	316.4±31.6	14.7±0.5
5*	3.9694			5	241.8	556.0±27.8	3.46±0.06
6*	4.9624			5	79.6	357.6±17.9	5.01±0.09

Second Lecture

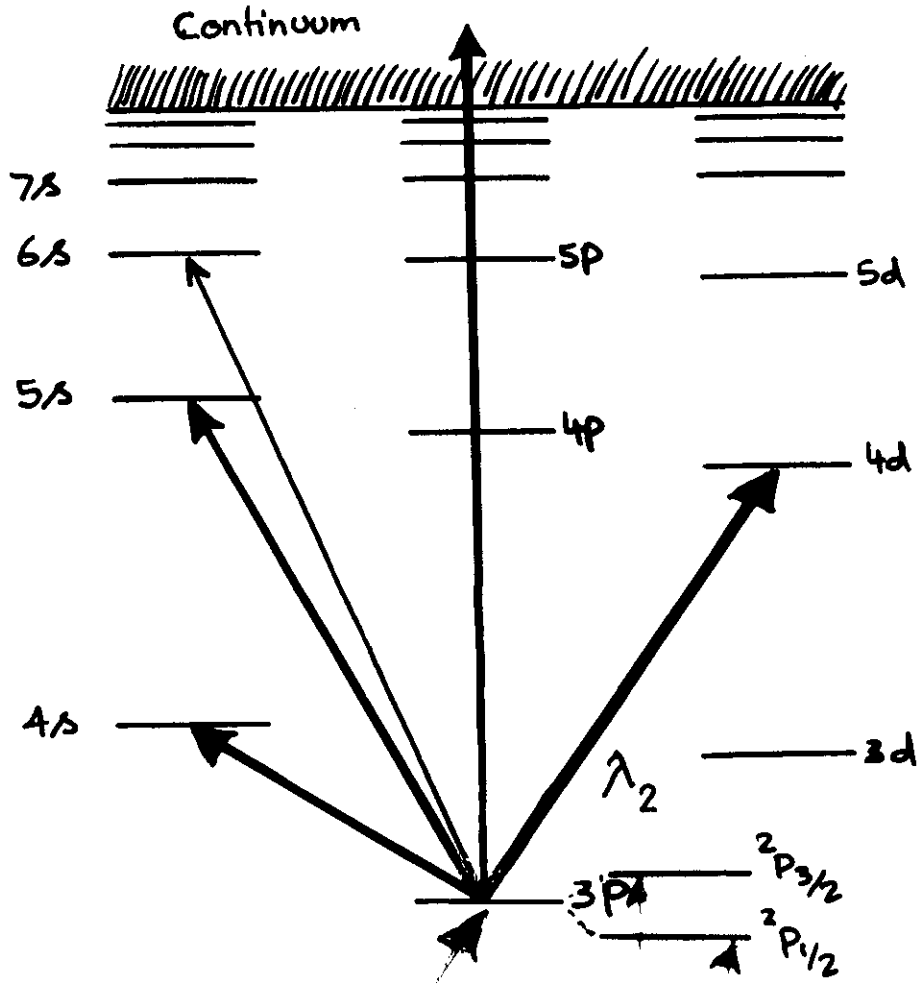
Continuum
7s
6s
5s
4s
5p
4p
3p
5d
4d
3d
λ_2
$^2P_{3/2}$
$^2P_{1/2}$
f=0.65
f=0.325
3s
$^2S_{1/2}$

Experimental setup

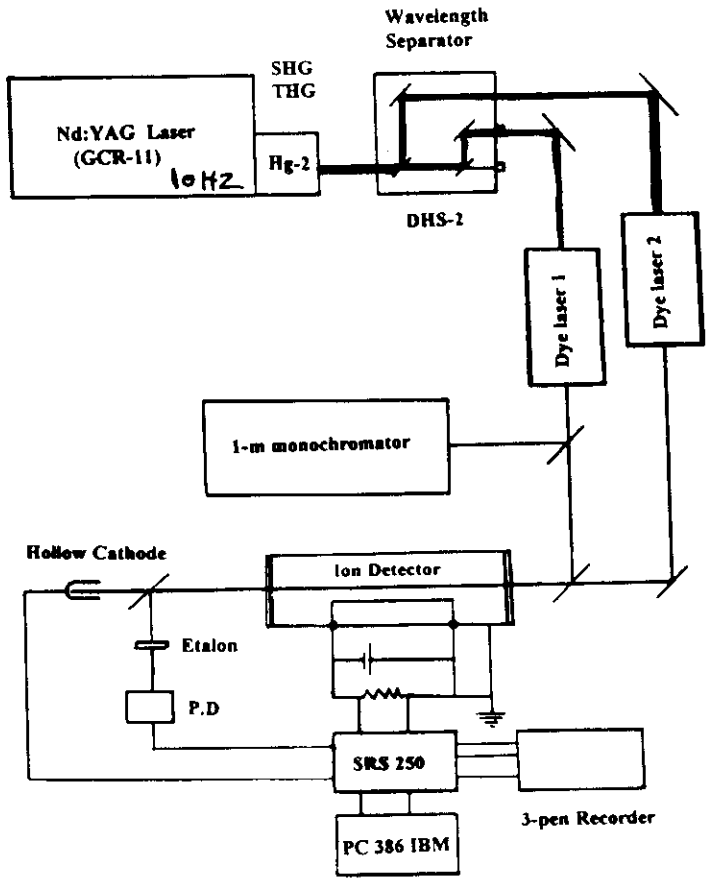

Na

Na_2

500K 3.39×10^{-2} 4.75×10^{-4} Torr

anode current = 3.5 Amp

Ar Buffer gas = 3 m Torr

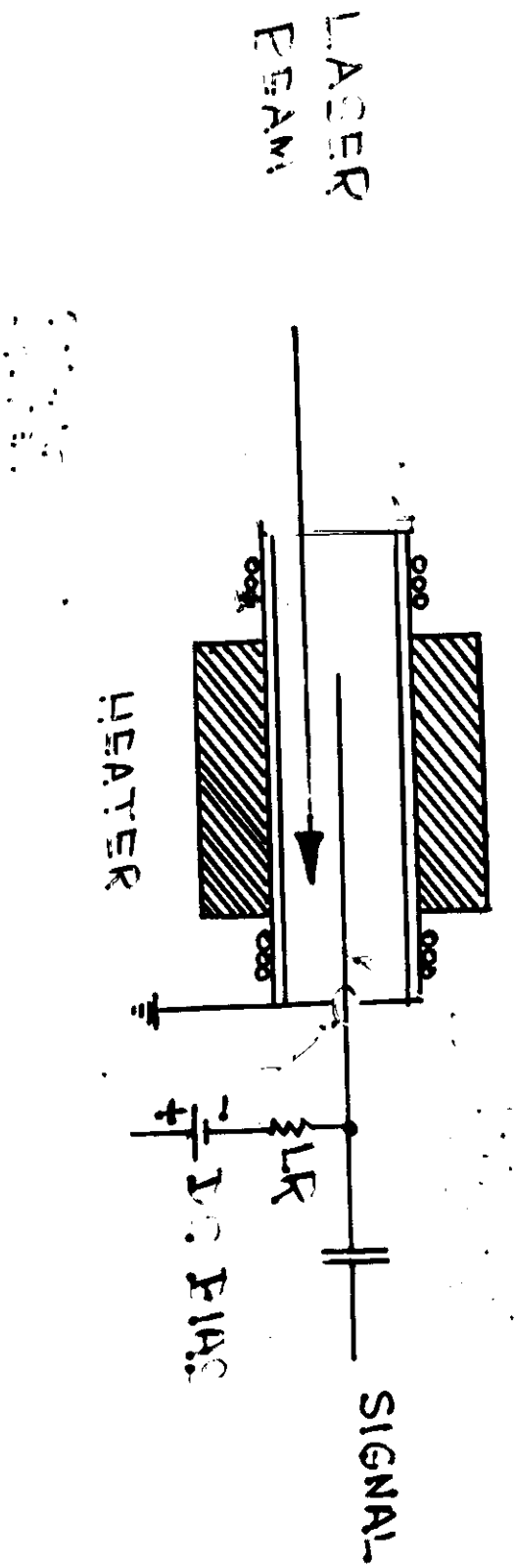
LASER BEAM
HEATER
SIGNAL

Cathode Current Dependence
(Temperature = 450 °C)

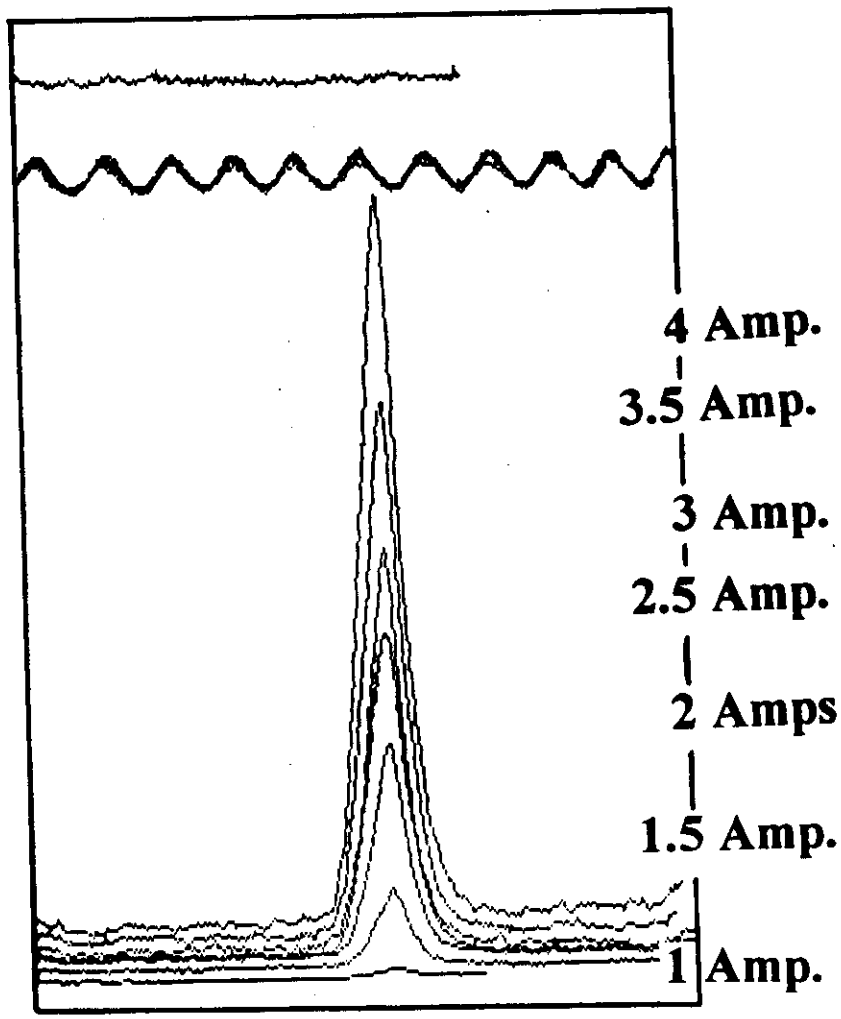

Lithium Resonance Transition (λ = 6710 Å)

$2s\ ^2S_{1/2} \rightarrow 2p\ ^2P_{3/2}$

Lithium Resonance Transition ($\lambda = 6710$ Å)

$2s\ ^2S_{1/2} \rightarrow 2p\ ^2P_{3/2}$

Vapor Pressure Dependence

(Cathode current = 2.8 Amp.)

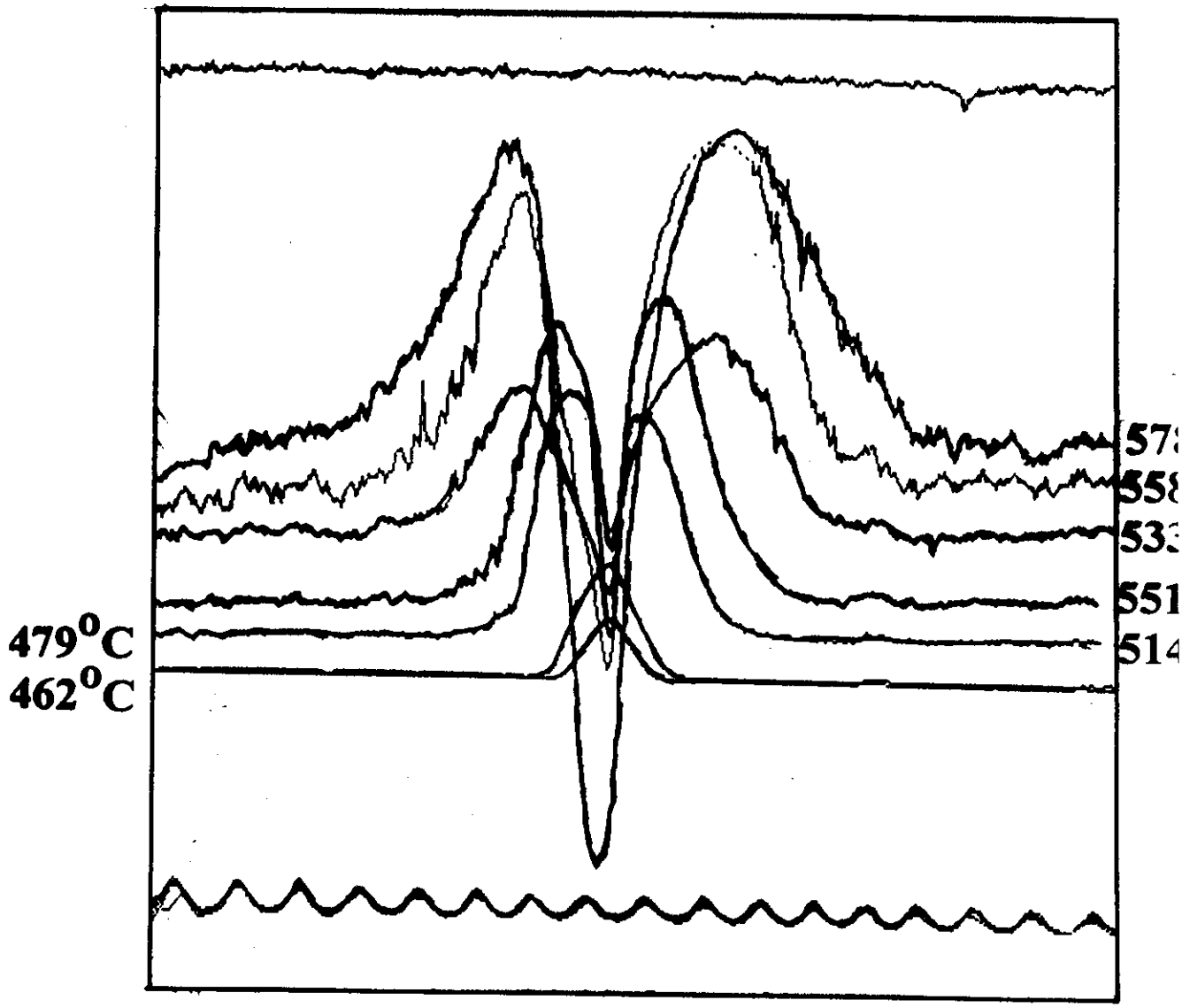

Energy Level Diagram of Lithium

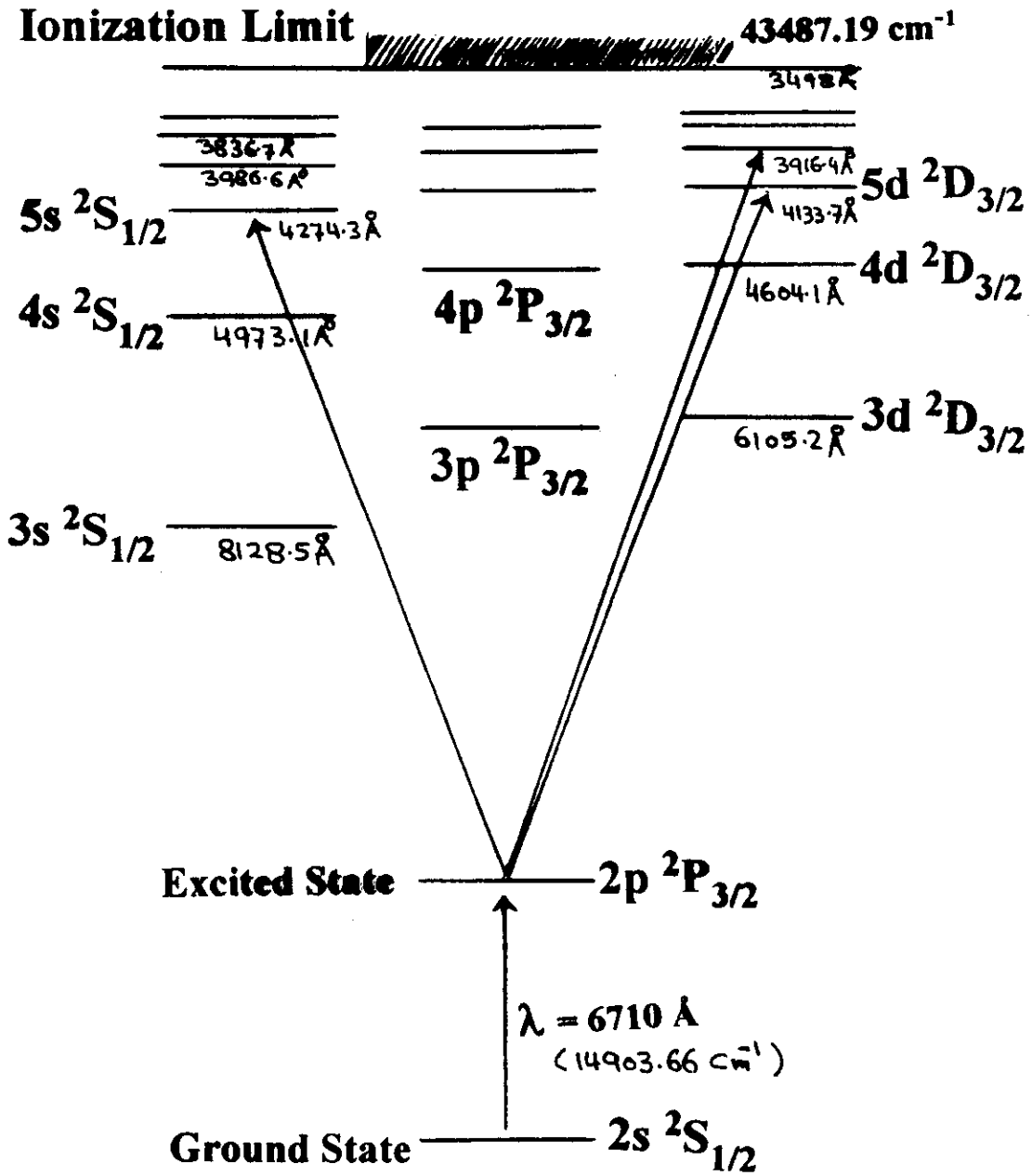

Two step Excitation NaI

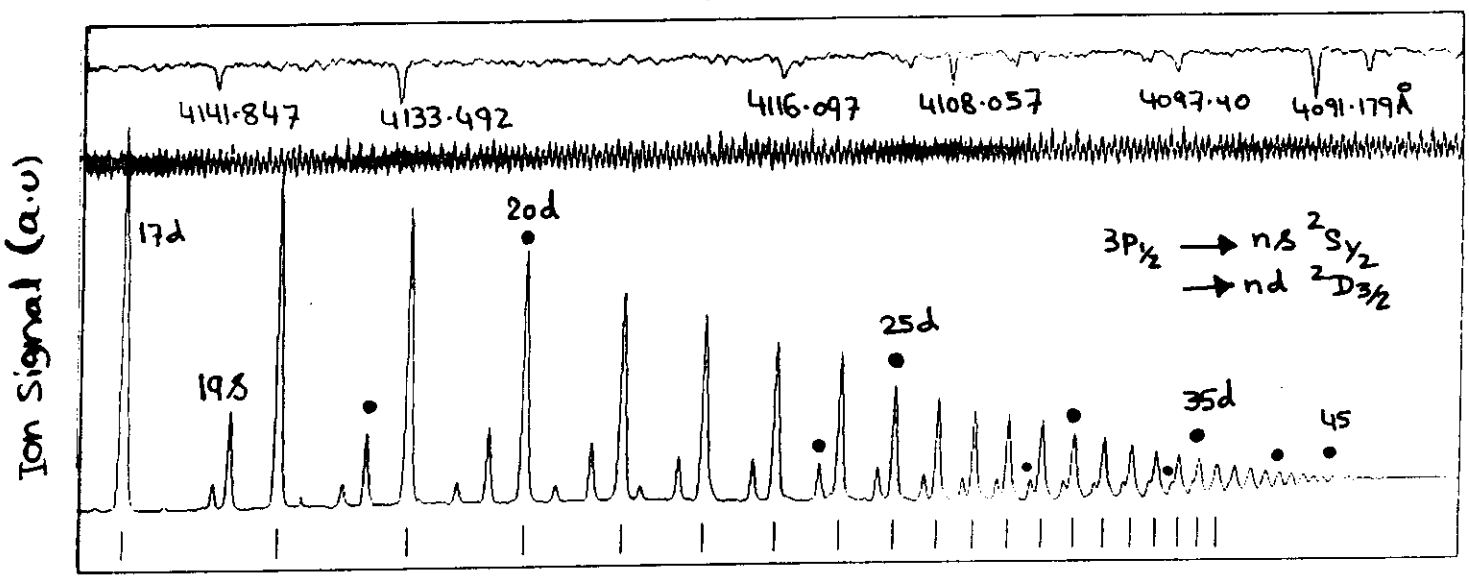

E. Dipole Transitions

$\Delta l = \pm 1$

$\Delta S = 0$

$\Delta J = 0, \pm 1$

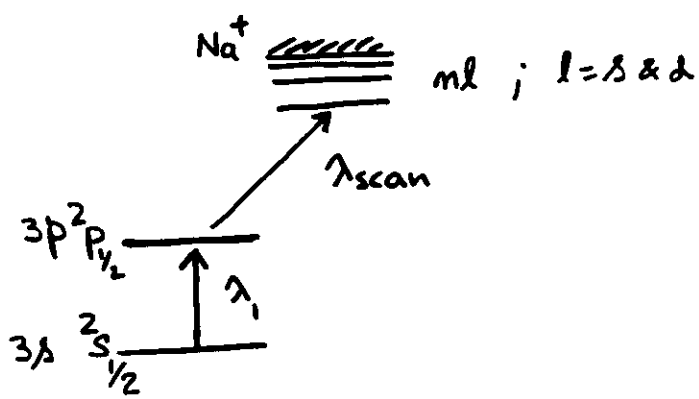

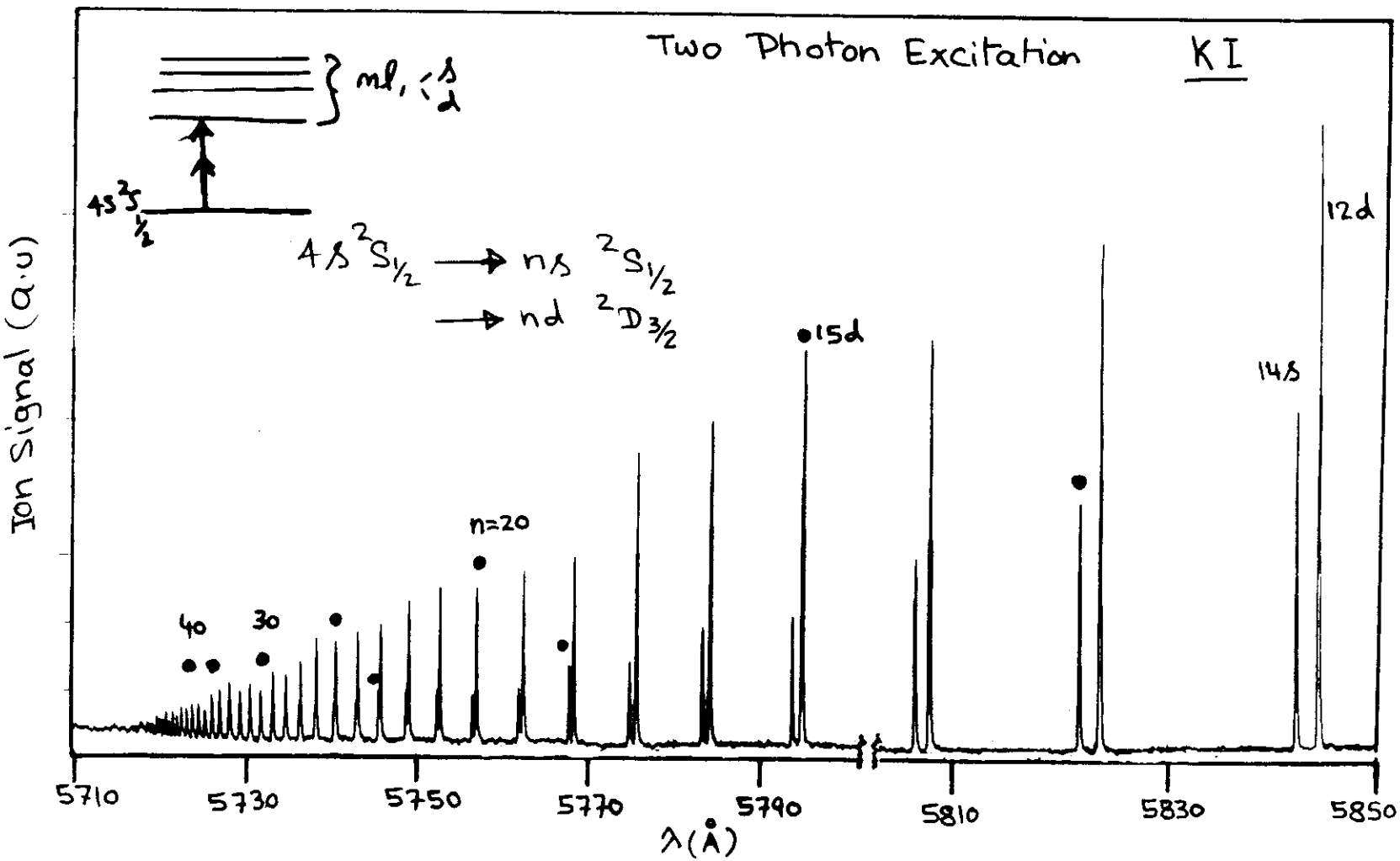
Two Photon Excitation
K I
nl, l = s, d
4s ²S½
4s ²S½ → ns ²S½
→ nd ²D3/2
Ion Signal (a.u)
n=20
15d
14s
12d
40
30
5710
5730
5750
5770
5790
5810
5830
5850
λ(Å)

Two Color Three Photon Resonance Ionization of Li

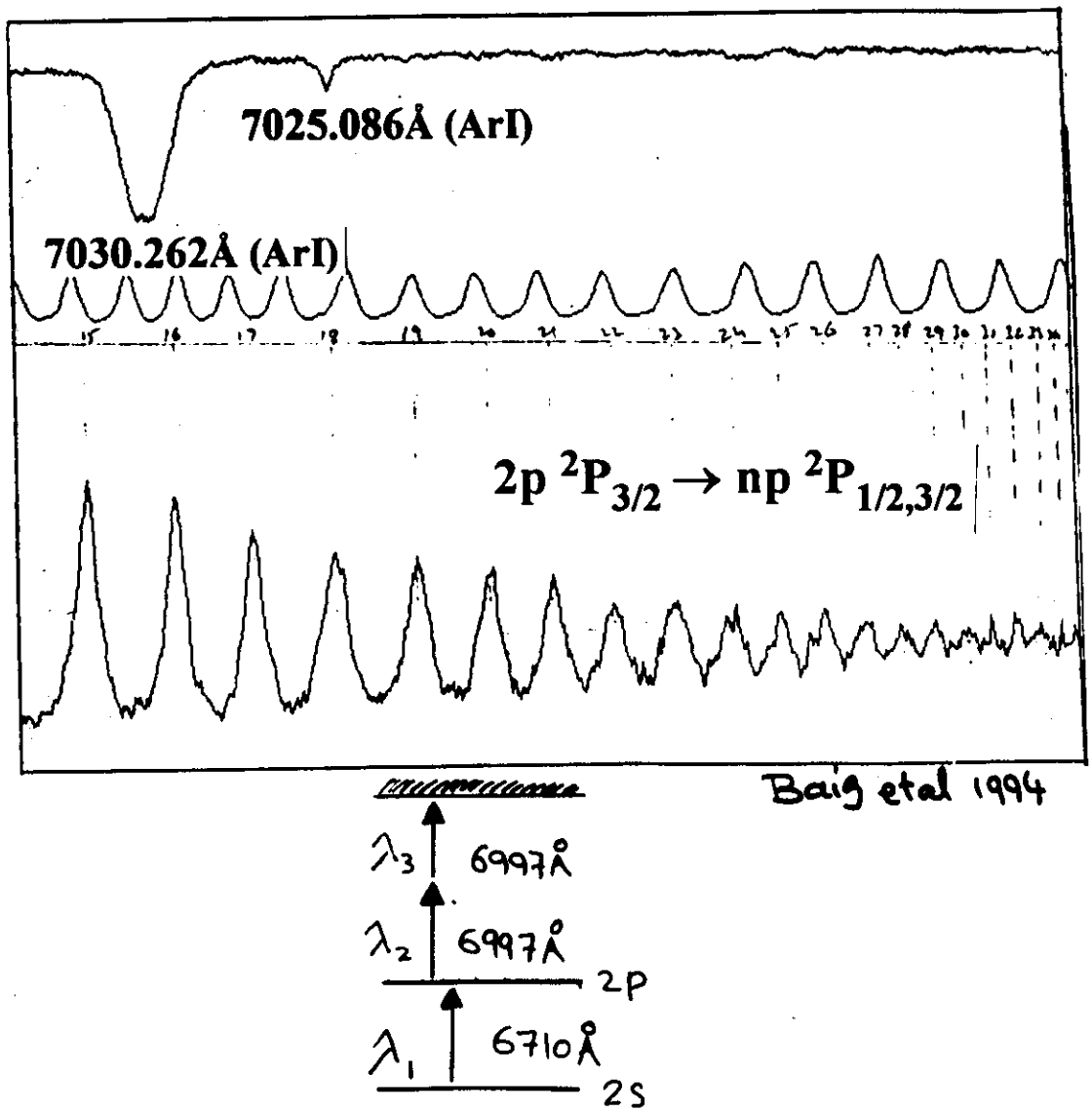

n-Photon Excitation

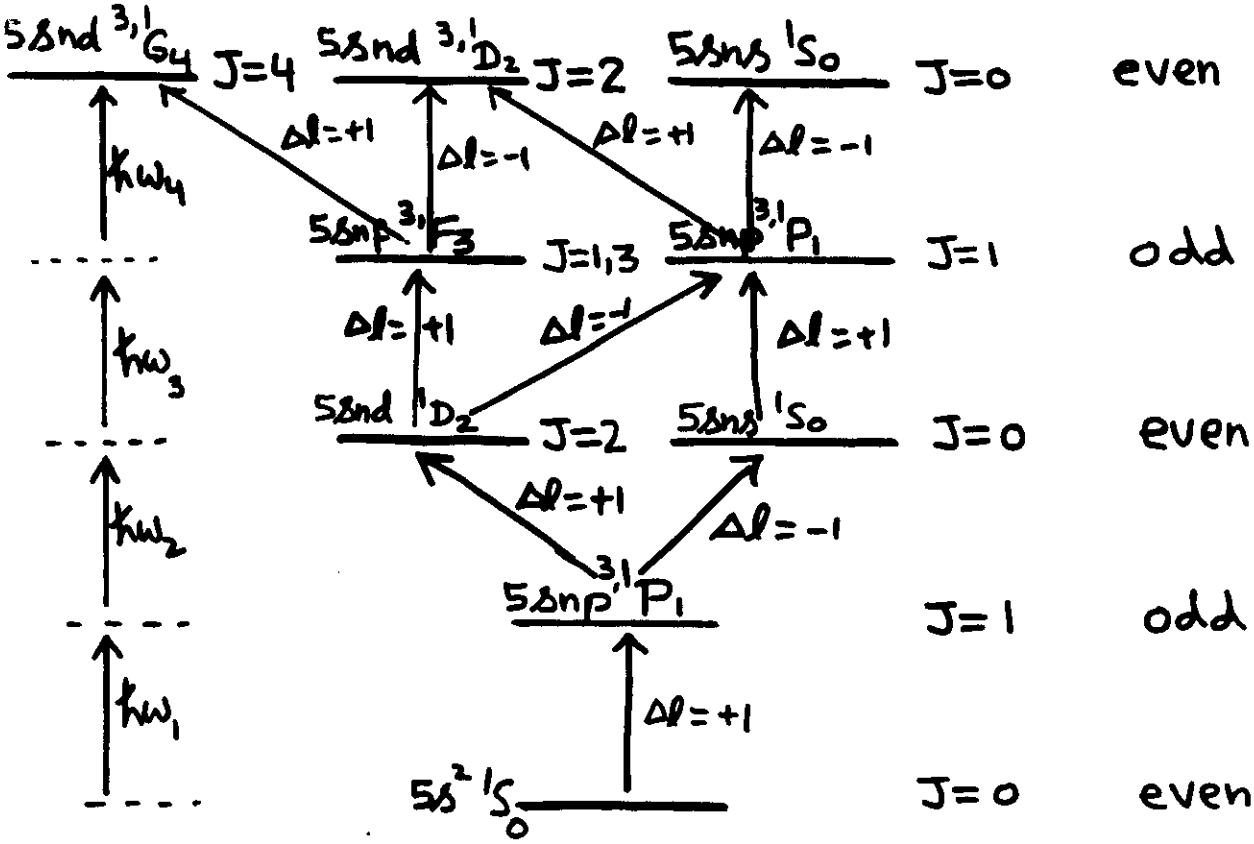

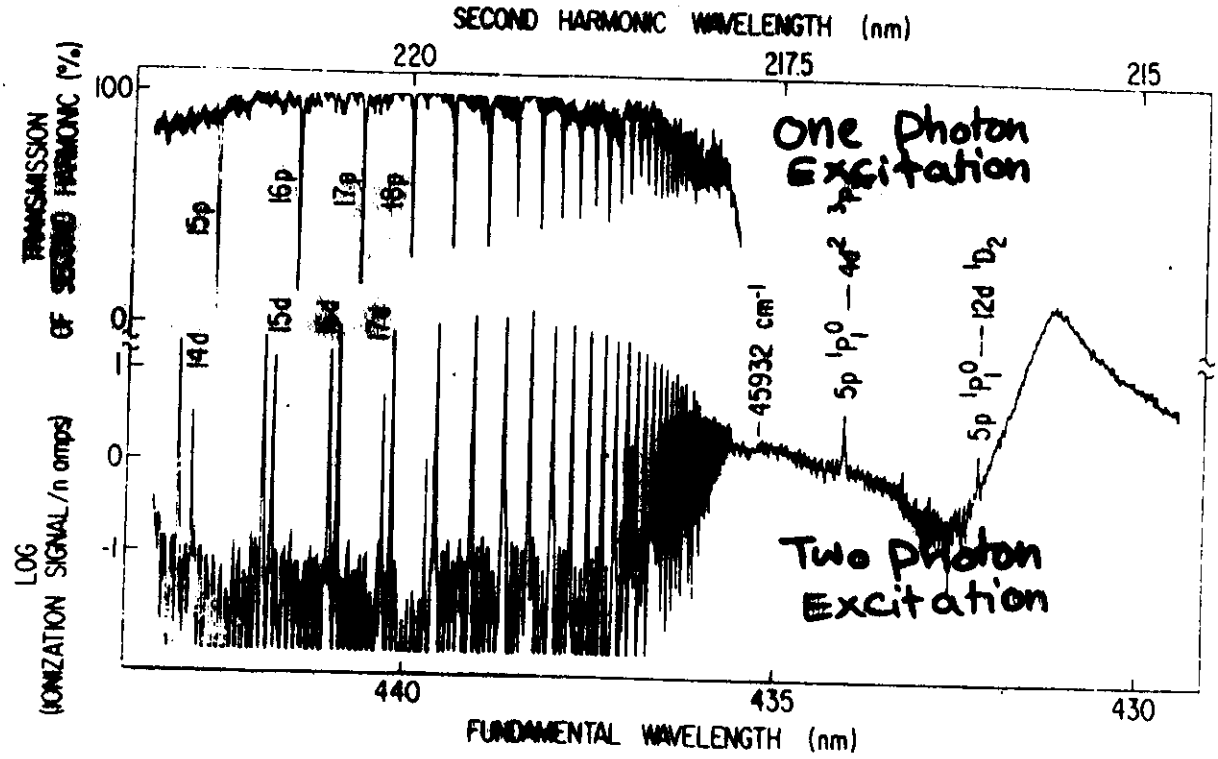
SECOND HARMONIC WAVELENGTH (nm)
220
217.5
215
100
0
-1
0
-1
TRANSMISSION OF SECOND HARMONIC (%)
LOG (IONIZATION SIGNAL/n amps)
15p
16p
17p
18p
14d
15d
45932 cm⁻¹
5p ¹P₁⁰ — 4d²
5p ¹P₁⁰ — 12d ¹D₂
One Photon Excitation
Two Photon Excitation
440
435
430
FUNDAMENTAL WAVELENGTH (nm)

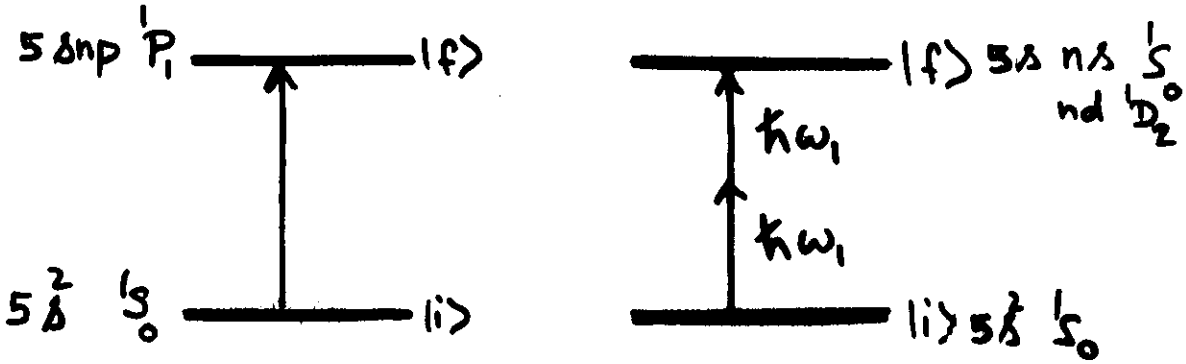
5 5np ¹P₁
|f⟩
5s² ¹S₀
|i⟩
|f⟩ 5s ns ¹S₀
nd ¹D₂
ħω₁
ħω₁
|i⟩ 5s² ¹S₀

Three Photon Excitation

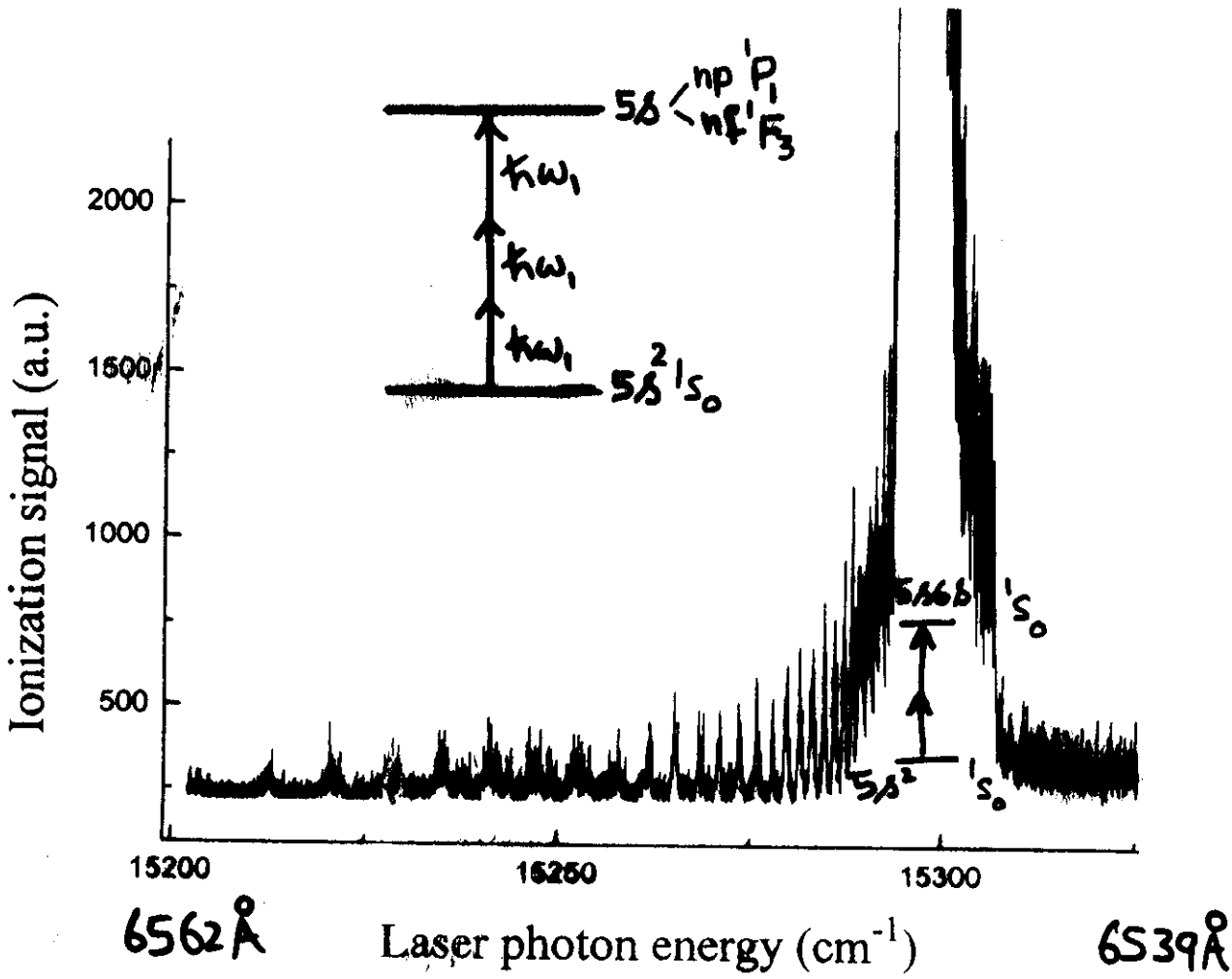

Selection rules

- Parity = odd
- Total Angular momentum = 1 & 3

Three Step Excitation

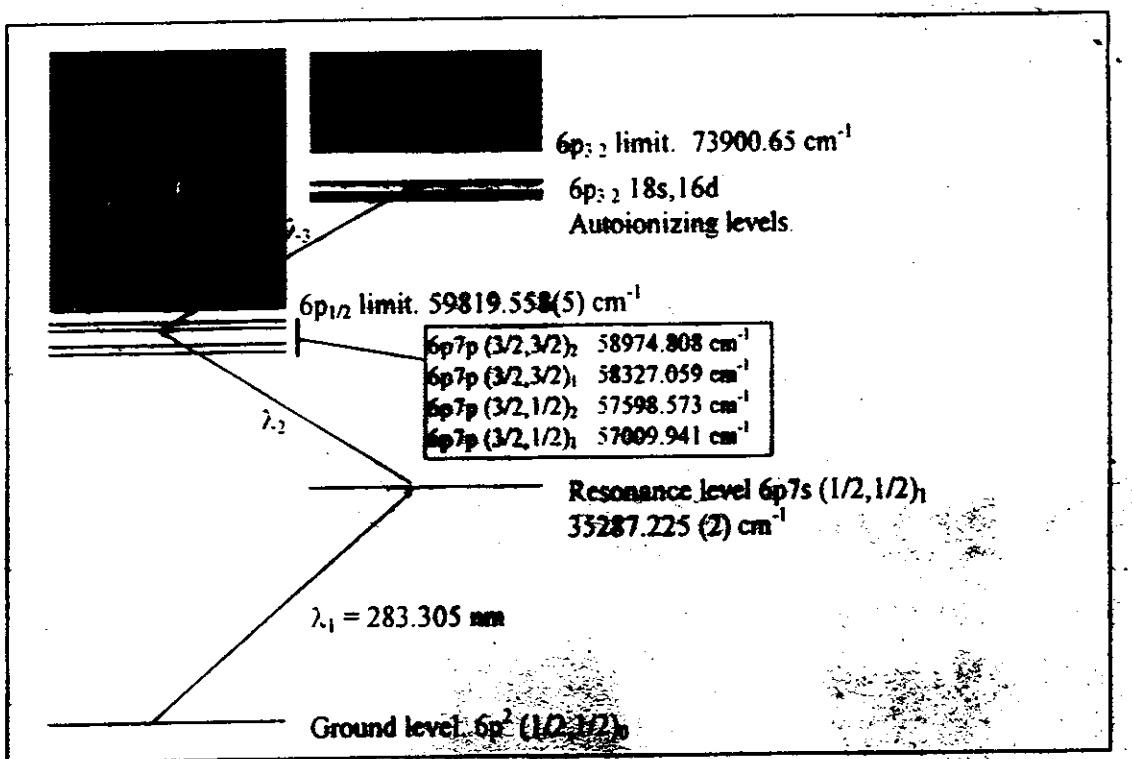

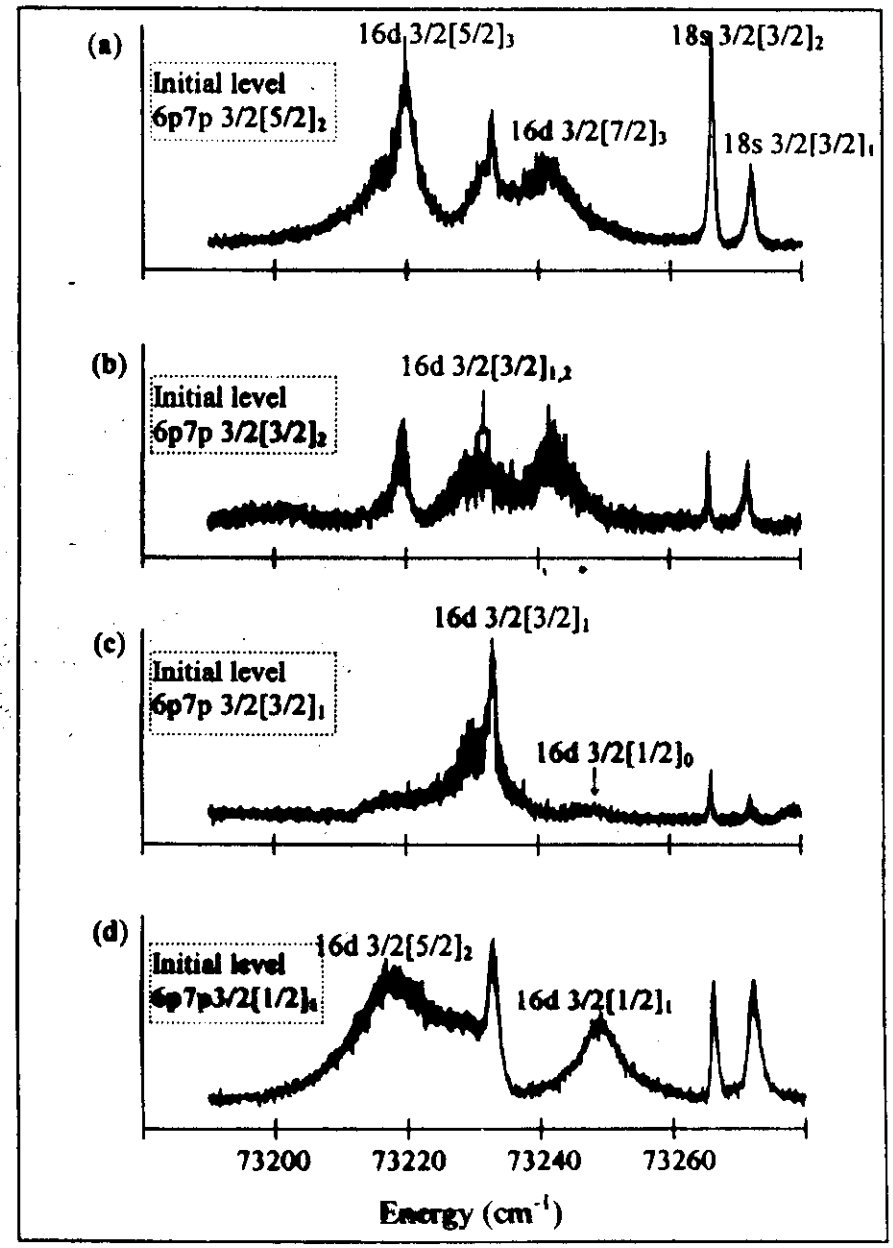

Bhatti et.al (1997) J. Phys. B:

Molecular Dissociation Energy

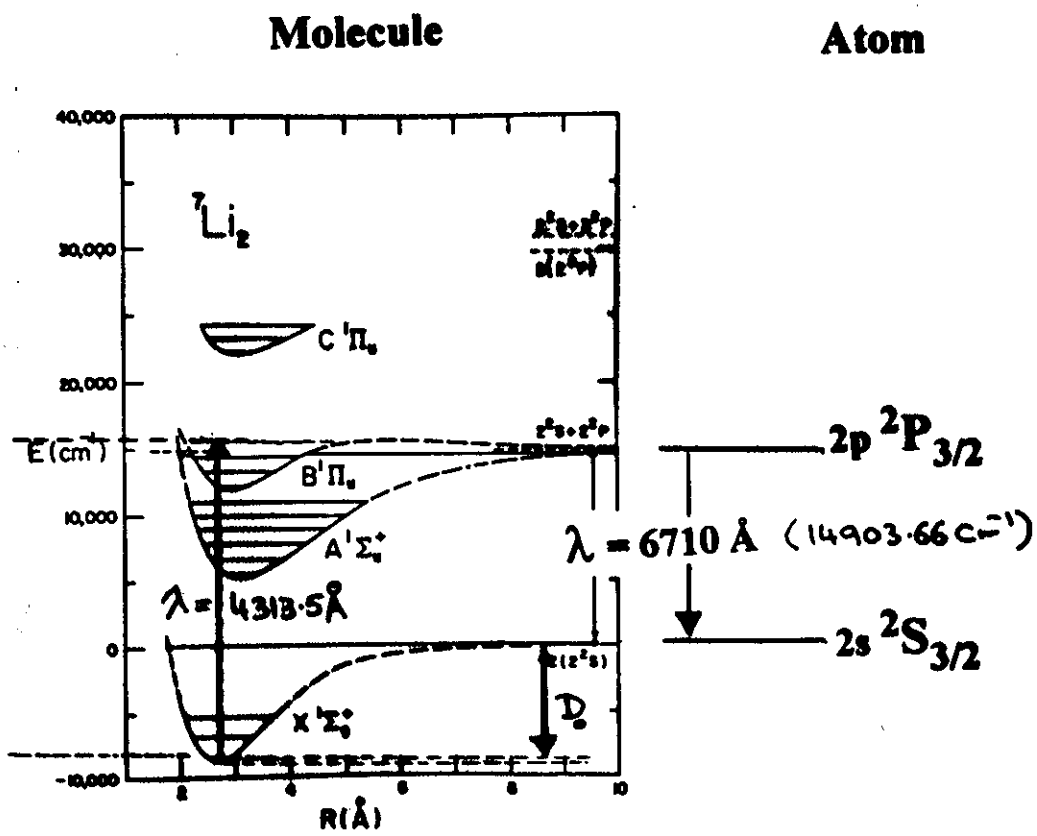

$$D_o'' = E_{\text{Molec}} - E_{\text{Atom}}$$

$$= 23183 - 14903.66$$

$$D_o'' = 8279 \pm 1\ \text{cm}^{-1}$$

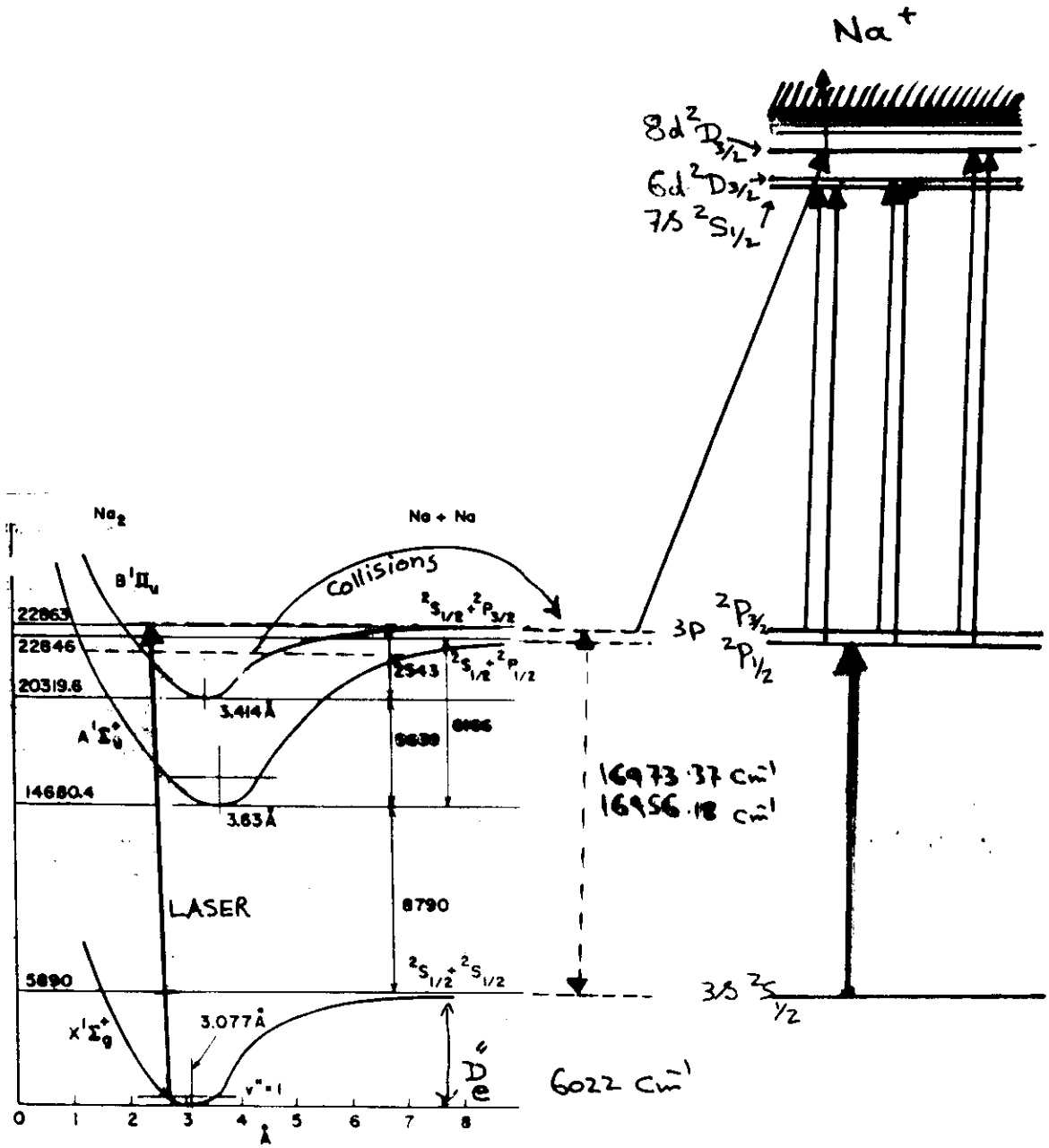
Na+
8d 2D3/2
6d 2D3/2
7s 2S1/2
Na2
Na + Na
B 1Πu
Collisions
2S1/2 + 2P3/2
2S1/2 + 2P1/2
3P 2P3/2
2P1/2
22863
22846
20319.6
14680.4
5890
3.414Å
3.63Å
3.077Å
A 1Σu+
X 1Σg+
2543
9639
8790
LASER
16973.37 cm-1
16956.18 cm-1
6022 cm-1
De
v"=1
3S 2S1/2
0 1 2 3 4 5 6 7 8
Å

Laser Induced Dissociation of Na_2

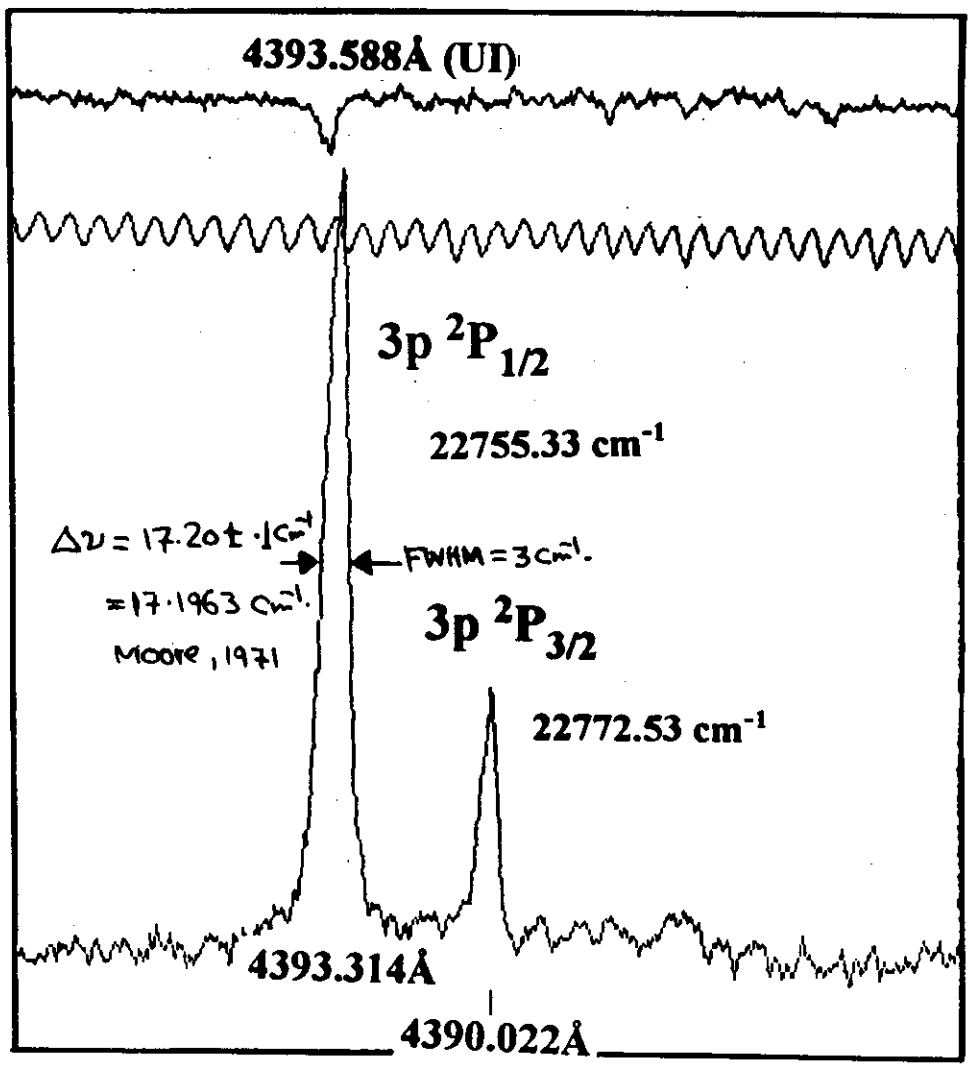

$$\frac{I(^2P_{1/2})}{I(^2P_{3/2})} = 2.9$$

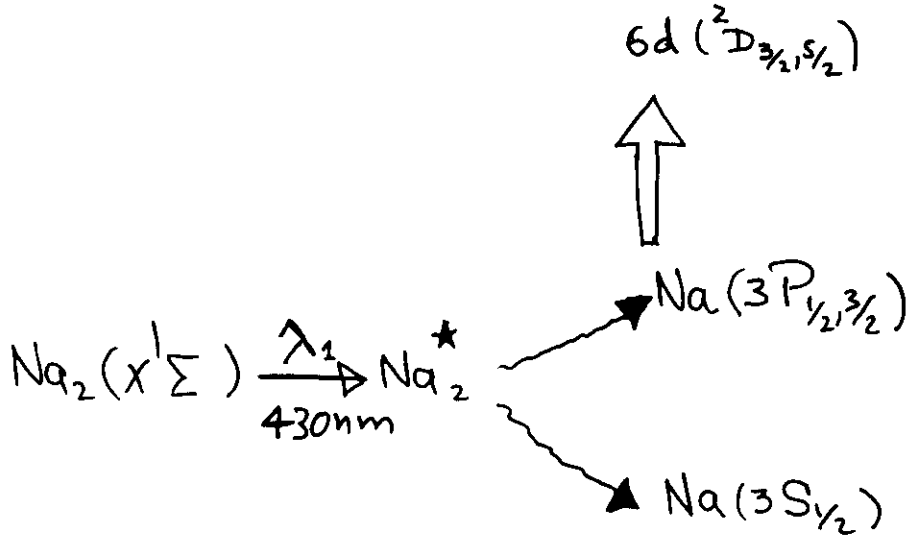

$3P_{1/2} \rightarrow 7S_{1/2}$ 21056 cm^{-1}

$3P_{3/2} \rightarrow 7S_{1/2}$ 21039 cm^{-1} ~ 475.3 nm

$3P_{1/2} \rightarrow 6d\ ^2D_{3/2}$ 21431

$3P_{3/2} \rightarrow 6d\ ^2D_{5/2}$ 21414 ~ 466.9 nm

$3P_{1/2} \rightarrow 8d\ ^2D_{3/2}$ 22772

$3P_{3/2} \rightarrow 8d\ ^2D_{5/2}$ 22755 ~ 439.5 nm

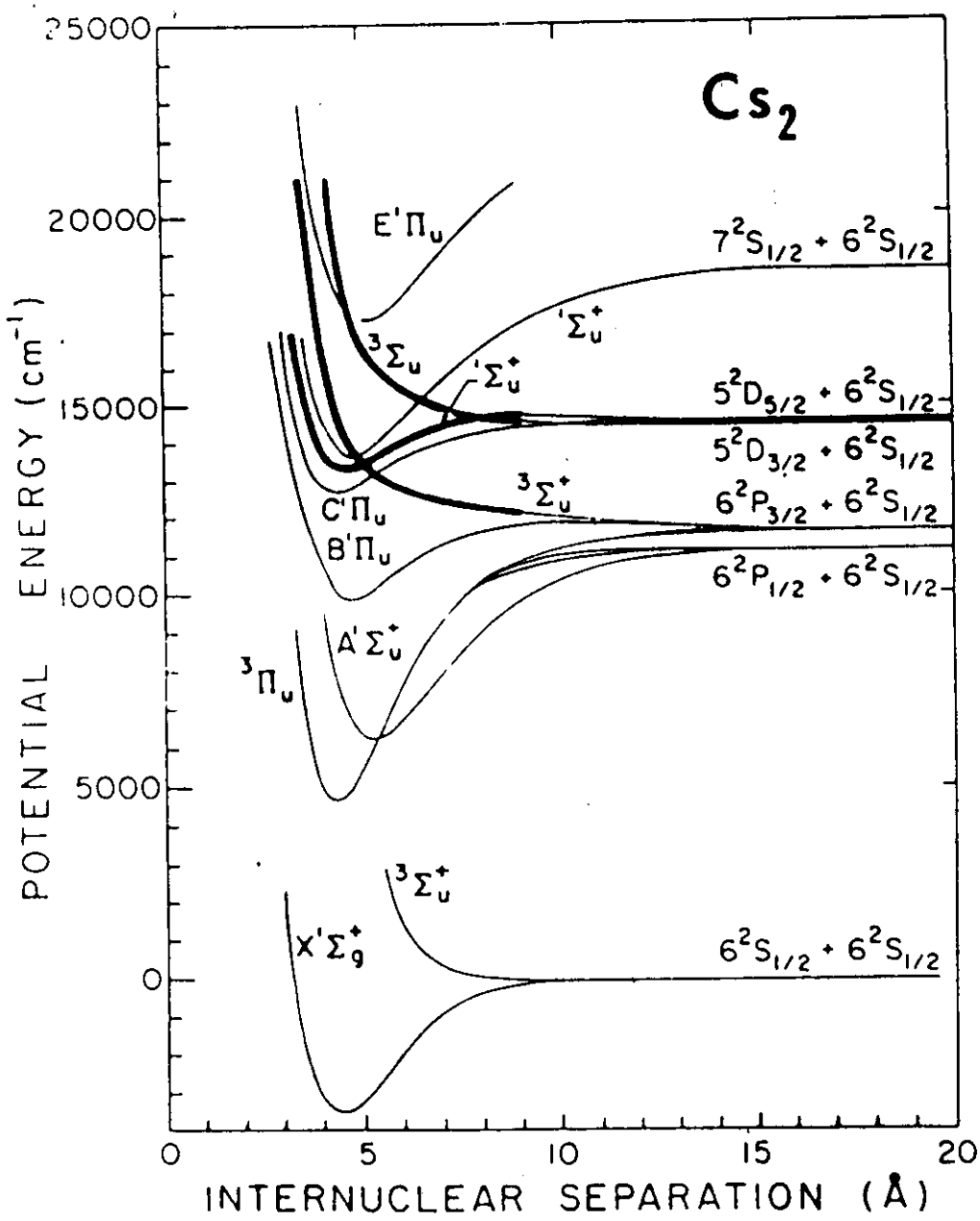

FIG. 3. Potential curves for the excited states of Cs_2. Light lines show potentials that were constructed from molecular constants obtained from the literature sources summarized in Table I. Heavy lines plot potentials approximated from the results of this work.

High-resolution photoabsorption measurement and multichannel quantum-defect-theory of the $2p^5 3s(^1P_1)$ ns,nd autoionizing series of sodium

M. A. Baig
Atomic and Molecular Physics Laboratory, Department of Physics, Quaid-I-Azam University, Islamabad, Pakis

S. A. Bhatti
Applied Physics Division, PINSTECH, P. O. Box Nilore, Islamabad, Pakistan

(Received 22 November 1993)

We measured the photoabsorption spectrum of sodium in the $2p$ subshell excitation region using synchrotron radiation and a 3-m spectrograph at a resolution of ±0.008 Å. In spite of the large number of overlapping structure due to the four ionization limits $2p^5 3s(^3P_{210}$ and $^1P_1)$, well separated autoionizing Rydberg series are detected converging to the $2p^5 3s(^1P_1)$ threshold. A three-channel quantum-defect-theory analysis is performed for the $2p^5 3s(^1P_1)ns$ and $2p^5 3s(^1P_1)nd$ autoionizing resonances. A simple n-channel multichannel quantum-defect-theory formula in terms of cofactors is presented for the calculation of the photoionization cross section for one open and $(n-1)$ bound channels.

PACS number(s): 32.30.Jc, 32.70.Jz, 32.80.Dz, 32.80.Fb

The $2p$ inner-shell excitation in sodium leads to four ionic states $2p^5 3s(^3P_{210}$ and $^1P_1)$ which serve as series limits for the Rydberg series according to the dipole-allowed photoabsorption from the $2p^6 3s(^2S_{1/2})$ ground state. Accordingly, there are four groups of Rydberg series converging on these pertinent ionic levels: four Rydberg series $2p^5 3s(^3P_2)$ $ns\,[2]^o_{3/2}$, $nd[0]^o_{1/2}$, $nd[1]^o_{1/2,3/2}$ and, $nd[2]^o_{3/2}$ to the $2p^5 3s(^3P_2)$ limit at 306 377.65 cm^{-1}, three series $2p^5 3s(^3P_1)$ $ns[1]^o_{1/2,3/2}$, $nd[1]^o_{1/2,3/2}$, $nd[2]^o_{3/2}$ to the $2p^5 3s(^3P_1)$ limit at 307 142.94 cm^{-1}, two series $2p^5 3s(^3P_0)$ $ns[0]^o_{1/2}$, $nd[2]^o_{3/2}$ to the $2p^5 3s(^3P_0)$ limit at 307 735.01 cm^{-1}, and three series $2p^5 3s(^1P_1)$ $ns[1]^o_{1/2,3/2}$, $nd[1]^o_{1/2,3/2}$, and $nd[2]^o_{3/2}$ to the $2p^5 3s(^1P_1)$ limit at 310 216.32 cm^{-1}. Due to the small spin-orbit interaction parameter $\zeta_p = 980$ cm^{-1} in the $2p^5 3s$ parent-ion configuration, the ^3P fine-structure levels lie very close in energy, whereas the ^1P level lies about 2481 cm^{-1} above the triplet levels. Consequently, the Rydberg series to the ^1P limit are well isolated in energy from the series to the ^3P limits. Indeed we have observed strong Rydberg series of ns and nd character to the $2p^5 3s(^1P_1)$ limit and very weak series to all the $2p^5 3s(^3P_{210})$ limits. Since all the observed transitions lie above the first ionization threshold, they can decay into the underlying $2p^6 \epsilon p$ continuum; as a result, the lines show Beutler-Fano- [1]type autoionizing resonances. We have observed the strongly autoionizing Rydberg series $2p^5 3s(^1P_1)nd$ up to $n=20$. The $2p^5 3s(^1P_1)ns$ series can be resolved from the nd series up to $n=15$, a considerable extension from the previous observation of these series up to $n=10$ and 5, respectively [2,3].

In this paper we present the analysis of the autoionizing $2p^5 3s(^1P_1)nd$ and $2p^5 3s(^1P_1)ns$ resonances to the $2p^5 3s(^1P_1)$ limit based on the phase-shifted reaction-matrix multichannel quantum-defect theory (MQDT) of Cooke and Cromer [4] and Giusti-Suzor and Fano [5]. We also present a simple n-channel MQDT expression in terms of cofactors to calculate the photoionization cross section for the case of one open and $(n-1)$ bound channels. The existing relations for calculating th ization cross section for one open and one bou [5] and one open and two bound channels [6 rived from the general MQDT formula.

The spectra were recorded in the first ord vacuum spectrograph equipped with a 50 holographic grating. The equipment is delivering a resolution of the order of 0.008 Å μm slit width and the reciprocal dispersion is at 400 Å. Synchrotron radiation emitted fro MeV electron accelerator provided the source of continuum. An absorption colum mately 1000 mm long was achieved by vapor lic sodium in a resistively heated furnace of ir ter 2 cm and 1 mm wall thickness. The f operated at temperatures in the range of which correspond to vapor pressure of sodiun to 1 Torr, respectively. The spectra were c energy by superposing the absorption spectra [9] and neon [10], both of which contain well- lines in the spectral region investigated in the periment.

The spectra were recorded on Kodak SWR exposure times ranging from 5 to 10 min. were measured on an Abbe comparator with accuracy of ±0.008 Å for sharp lines. The curve was fitted by a third-order Chebyschev to an internal consistency of ±0.002 Å. T recorded on the photographic plates were digi computer-controlled microdensitometer in st using a slit width of 10 μm at the photomul

A densitometer trace of the photoabsorp is presented in Fig. 1, which shows the ove ture of Rydberg series in the vicinity of limits, marked as arrows. The observed to the $2p^5 3s(^1P_1)$ singlet-based limit are whereas the series to the $2p^5 3s(^3P_{210})$ trip are too weak to be detected near the lim feature of the observed $2p^5 3s(^1P_1)ns$ and

the *nd* lines have broad, typical Beutler-Fano profiles, whereas the *ns* lines are relatively sharp, a close similarity with the autoionizing Rydberg series observed in inert gases [10–15], where the $mp^5(^2P_{1/2})$ ($m=2$, 3, 4, and 5 for neon, argon, krypton, and xenon, respectively) based $[3/2]_1$ series show autoionization and the $ns[1/2]_1$ lines remain sharp. Another interesting observation is that the $2p^53s(^1P_1)6d$ line, which lies just above the $2p^53s(^3P_2)$ limit, shows pronounced autoionization effect, whereas the adjacent lower member of this series $2p^53s(^1P_1)5d$, which lies below the $2p^53s(^3P_2)$ limit, exhibits very strong and sharp resonance. The $2p^53s(^1P_1)7s$ line also shows some broadening effects but remains relatively sharp (see Fig. 1). This abrupt change in the line shapes of the *nd*-series members across the $2p^53s(^3P_2)$ limit indicates that the $2p^53s(^1P_1)nd$ channel is strongly coupled to the $2p^53s(^3P_2)\varepsilon l$ open channel and only weakly coupled to the $2p^6(^1S_0)\varepsilon p$ channel. The coupling of the $2p^53s(^1P_1)ns$ series lines to the $2p^53s(^3P_2)\varepsilon l$ open channel is small and, consequently, the lines of the $2p^53s(^1P_1)ns$ Rydberg series remain sharp.

In order to analyze the line shapes of the observed autoionizing resonances, we have used the phase-shifted multichannel quantum-defect theory reaction-matrix formalism given by Cooke and Cromer [4]. The MQDT equation takes a matrix form

$$\mathbf{a}=0 , \tag{1}$$

where $\mathbf{K}$ is the interaction matrix whose diagonal elements are zero, the off-diagonal elements R_{ij} describe the coupling between the ith and jth channels, and ε is the diagonal matrix whose components for the bound channels are as

$$\tan[\pi(\nu_i+\mu_i)] , \tag{2}$$

where μ_i is the quantum defect, ν_i is the effective quantum number of the ith bound channel with respect to the ionization threshold, $\nu_i=[\mathrm{Ry}/(I_i-E_n)]^{1/2}$, and $\mathbf{a}$ is the column vector given as

$$a_i=A_i\cos[\pi(\nu_i+\mu_i)] , \tag{3}$$

where A_i are the amplitudes of the ith dissociation channel. For the open channels ε_{ij} are the phase shifts which are equal to ε_0 and $\mathbf{a}$ is normalized such that

$$\sum_0 a_0^2=[1+\varepsilon_0^2]^{-1} . \tag{4}$$

In the autoionization region the atomic spectra can be well described by one generalized continuum and $(n-1)$ bound channels. The MQDT compatibility equation takes a particularly simple form:

$$\begin{pmatrix} \varepsilon_1 & R_{12} & R_{13} & \cdots & R_{1n} \\ R_{12} & \varepsilon_2 & R_{23} & & R_{2n} \\ R_{13} & R_{23} & \varepsilon_3 & & R_{3n} \\ & & & & \\ R_{1n} & R_{2n} & R_{3n} & & \varepsilon_n \end{pmatrix} \begin{pmatrix} a_1 \\ a_2 \\ a_3 \\ \\ a_n \end{pmatrix} = 0 . \tag{5}$$

Considering channel 1 open and channels from 2 to n as bound, a nontrivial solution of the MQDT equation (5) requires the determinant of the coefficient matrix to vanish. The determinant is equal to

$$\varepsilon_1 C_{11}+\sum_2^n R_{1i}C_{1i}=0 . \tag{6}$$

Here the determinant has been expanded by the first row and the summation is over the bound channels. The C_{1i} are the cofactors of the first row of the MQDT matrix. This immediately yields

$$\varepsilon_1=-(1/C_{11})\sum_2^n R_{1i}C_{1i} . \tag{7}$$

Substituting it in the normalization condition for the open channel, $a_1^2=[1+\varepsilon_1^2]^{-1}$, it yields

$$a_1^2=C_{11}^2\Big/C_{11}^2+\left|\sum_2^n R_{1i}C_{1i}\right|^2 . \tag{8}$$

The next step is to write the last $(n-1)$ equations in the matrix form

$$\begin{pmatrix} \varepsilon_2 & R_{23} & \cdots & R_{2n} \\ R_{23} & \varepsilon_3 & & R_{3n} \\ & & & \\ R_{2n} & R_{3n} & & \varepsilon_n \end{pmatrix} \begin{pmatrix} a_2/a_1 \\ a_3/a_1 \\ \\ a_n/a_1 \end{pmatrix} = - \begin{pmatrix} R_{12} \\ R_{13} \\ \\ R_{1n} \end{pmatrix} . \tag{9}$$

The quantities we will need are the square of the ratio of the amplitudes in the dissociation channels. All the (a_i/a_1) can be calculated from the above relation using the Cramer's rule for solving the set of simultaneous inhomogeneous equations:

$$a_i/a_1=-C_{1i}/C_{11} . \tag{10}$$

The denominator determinant is the cofactor C_{11}, while the numerator is the cofactor C_{1i} with the negative sign.

The photoionization cross section is calculated using the expression [4–7]

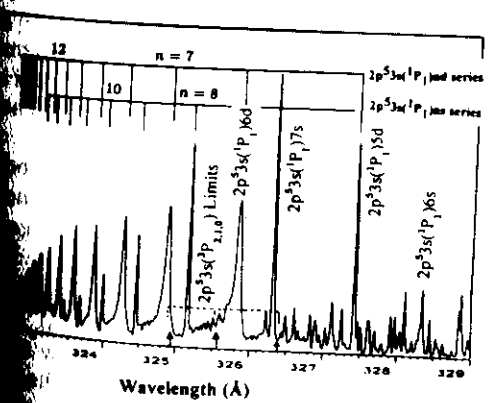

Photometer trace of the photoabsorption spectrum in the region between 290–320 Å showing oscillatory series to all the four limits of the $2p^53s$ configuration. The ionization thresholds $2p^53s(^3P_{210})$ are shown by arrows. The change in the linewidth of the resonance in the adjacent member $2p^53s(^1P_1)6d$ is seen near the $2p^53s(^3P_2)$ threshold.

$$\sigma = K \left| \sum_1^n a_i D_i \right|^2 , \tag{11}$$

where $K = 4\pi^2 \alpha \hbar\omega$ which does not change appreciatively over the energy range covered by a typical single-photon autoionizing spectra. Here $\hbar\omega$ is the photon energy and α is the fine-structure constant. The short-range parameters D_i are the transition dipole moments between the initial state and the ith channel. Substituting the values of a_i in this equation, the photoionization cross section can be expressed as

$$\sigma = K(a_1^2 / C_{11}^2) \left| \sum_1^n C_{1i} D_i \right|^2 . \tag{12}$$

Incorporating the value of the a_1^2 from Eq. (8) in the above relation, a generalized expression for the photoionization cross section with one open and $(n-1)$ bound channels is obtained:

$$\sigma = K \left| \sum_1^n C_{1i} D_i \right|^2 \Big/ C_{11}^2 + \left| \sum_2^n C_{1i} R_{1i} \right|^2 . \tag{13}$$

Note that the summation in the numerator is over all the n channels involved, while in the denominator the summation is only over the $(n-1)$ bound channels.

From this general expression, we can derive the existing relations [4,5] to calculate the photoionization cross section. The simplest case is with one open and one bound channel. The MQDT matrix for this situation is

$$\begin{vmatrix} \varepsilon_1 & R_{12} \\ R_{12} & \varepsilon_2 \end{vmatrix} ,$$

where $\varepsilon_2 = \tan[\pi(\nu_2 + \mu_2)]$. The cofactors of th are $C_{11} = \varepsilon_2$ and $C_{12} = -R_{12}$. Substituting thes the expression (13), the relation for the phot cross section becomes

$$\sigma = K \frac{\left| \tan[\pi(\nu_2+\mu_2)] D_1 - R_{12} D_2 \right|^2}{\tan^2[\tan(\nu_2+\mu_2)] + R_{12}^4} .$$

This is the same expression as derived by Gi and Fano [5] and Cooke and Cromer [4].

For the three-channel problem, one open bound channels, the MQDT matrix is

$$\begin{vmatrix} \varepsilon_1 & R_{12} & R_{13} \\ R_{12} & \varepsilon_2 & R_{23} \\ R_{13} & R_{23} & \varepsilon_3 \end{vmatrix} ,$$

where $\varepsilon_2 = \tan[\pi(\nu_2+\mu_2)]$ and $\varepsilon_3 = \tan[\pi(\nu_3+\mu$ cofactors of the first row are

$$C_{11} = (\varepsilon_2\varepsilon_3 - R_{23}^2), \quad C_{12} = -(\varepsilon_3 R_{12} - R_{13}R_{2}$$

$$C_{13} = -(\varepsilon_2 R_{13} - R_{12}R_{23}) .$$

The photoionization cross-section expression is becomes

$$\sigma = K \frac{|(\varepsilon_2\varepsilon_3 - R_{23}^2)D_1 - (\varepsilon_3 R_{12} - R_{13}R_{23})D_2 - (\varepsilon_2 R_{13} - R_{12}R_{23})D_3|^2}{(\varepsilon_2\varepsilon_3 - R_{23}^2)^2 + |(\varepsilon_2 R_{13}^2 + \varepsilon_3 R_{12}^2 - 2R_{12}R_{13}R_{23})|^2} .$$

This expression is identical to but much simpler than the relation derived by Giusti-Suzor and Lefebvre-Brion [6], Ueda [7], and Hieronymus, Neukammer, and Rinneberg [8]. One can similarly write the expressions for the $(n-1)$ bound channels interacting with one open channel. The main advantage of the general expression for calculating the photoionization cross section in terms of cofactors [Eq. (13)] is that the computer code remains as simple as for the one open and one bound channel problem.

For the quantitative analysis of the observed autoionizing resonances, the generalized quantum-defect-theory expression (13) was used for three channels. The open channel is $2p^5 3s(^3P_2)\varepsilon l$ and the two bound channels are $2p^5 3s(^1P_1)ns$ and $2p^5 3s(^1P_1)nd$, respectively. There also exists the $2p^6(^1S_0)\varepsilon p$ open channel which should be taken into account for the MQDT analysis. However, the energy difference between the $2p^6(^1S_0)$ threshold and the $2p$ inner-shell excitation structure is about 30 eV; therefore, its contribution can be neglected. Furthermore, there is no observed background due to the direct excitation in the $2p^6(^1S_0)\varepsilon p$ continuum channel (see Fig. 1). The two Rydberg series $2p^5 3s(^1P_1)ns$ and $2p^5 3s(^1P_1)nd$ both terminate to the same ionization threshold; thus, $I_2 = I_3 = 310\,212.2$ cm^{-1}. The quantum defects calculated with respect to the ionization limit are 0.618 ± 0.008 and 0.275 ± 0.008 for the ns and the nd series, respectively, which remain nearly constant, an indication of a ble interchannel interaction among these bound c thus, we put $R_{23} = 0$.

The results of our calculations are presented i The upper curve shows the calculated spectrum parameters given in Table I and the lower curv the experimentally observed spectrum. We have experimental bandwidth of about 5 cm^{-1} for a the calculated data. The calculated spectrum sho markable reproduction of the experimental spectr demonstrates the power of the MQDT to analyze toionizing resonances.

From the parameters in Table I it can be seen coupling of the $2p^5 3s(^1P_1)nd$ series to the $2p^5 3$ open channel is nearly three times stronger than the $2p^5 3s(^1P_1)ns$ series. The observed widths (fu at half maximum) of the $2p^5 3s(^1P_1)6d$ resonance Å (110 ± 10 cm^{-1}) and that of the $2p^5 3s(^1P_1)7s$ re at 326.3 Å (40 ± 10 cm^{-1}) also follow a similar These parameters can be extended in the discrete below the $2p^5 3s(^3P_2)$ threshold by using the L graphical technique [16] as has been done in bariu There are at least 12 possible overlapping Rydber in this region: three nd and one ns series built $2p^5 3s(^3P_2)$ limit, two nd and one ns series built $2p^5 3s(^3P_1)$ limit, one nd and one ns series built $2p^5 3s(^3P_0)$ limit, and two nd and one ns series b

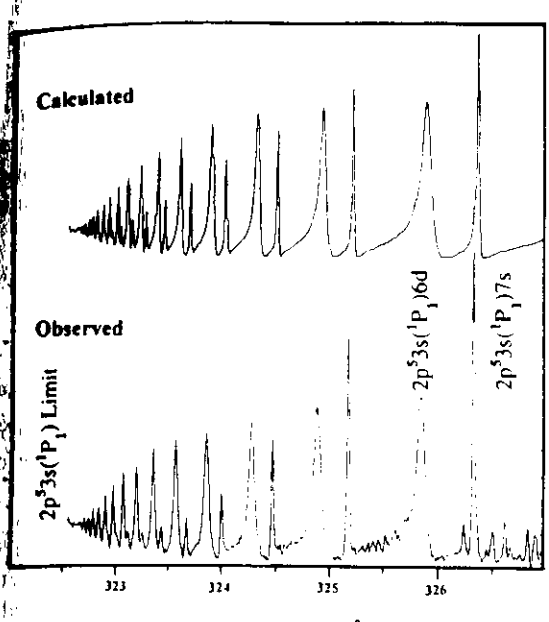

2. The calculated and the observed $2p^5 3s(^1P_1)ns,nd$ of autoionizing resonances in the absorption spectrum of covering the spectral region between 322–327 Å. The parameters used to reproduce the observed structure in Table I. An experimental bandwidth of 5 cm^{-1} was to average the calculated spectra in order to match the ob- spectrum.

$2p^5 3s(^1P_1)$ limit, within the framework of the $J_c K$-pling scheme [18,19]. The interchannel interactions ong these overlapping resonances seems to perturb the trum. In order to extract some meaningful parame- and a reliable interpretation, one must include all e channels in the MQDT analysis. We have not been to perform this extensive analysis because of the k nature of the observed structure in this region. A vestigation of this part of the spectrum at a higher rsion and resolution will be very beneficial for ex- ing the MQDT analysis.

n the inert gases, the $(^2P_{1/2})nd[3/2]_1$ series shows ltier-Fano–type autoionizing resonances because the uantum number in the $(^2P_{3/2})\varepsilon d[3/2]_1$ continuum channel and the discrete channel is identical. The $(^2P_{1/2})ns[1/2]_1$ series remains sharp because the K quantum numbers differ in the discrete and the $(^2P_{3/2})\varepsilon s[3/2]_1$ continuum channels. The situation in sodium is more complicated due to the existence of four thresholds as a result of the fine-structure splitting in the $2p^5 3s$ parent-ion configuration. An analogous analysis, therefore, cannot be extended for the interpretation of the autoionization in the $2p^5 3s(^1P_1)nd$ series in sodium because numerous open channels $2p^5 3s(^3P_{2,1,0})\varepsilon s$ and εd possessing $K=[1]_{1/2,3/2}$ and $[2]_{3/2}$ are present which can cause autoionization for both the $2p^5 3s(^1P_1)nd[1]_{1/2,3/2}$, and the $2p^5 3s(^3P_1)ns[1]_{1/2,3/2}$ series. The reason only the $2p^5 3s(^1P_1)nd$ series is broadened and the $2p^5 3s(^1P_1)ns$ series remains relatively sharp is not clear.

TABLE I. Three-channel MQDT parameters for the analysis of the autoionizing $2p^5 3s(^1P_1)ns,nd$ Rydberg series in sodium.

i,j	1	2	3
$\|i\rangle$	$2p^5 3s(^3P_2)\varepsilon l$	$2p^5 3s(^1P_1)ns$	$2p^5 3s(^1P_1)nd$
		$R_{12}=0.13$	$R_{13}=0.35$
			$R_{23}=0$
μ_i	0	0.618	0.275
D_i	−3.0	2.2	4
I_i	306 377.6 cm^{-1}	310 212.2 cm^{-1}	310 212.2 cm^{-1}

In conclusion, we have demonstrated that the $2p^5 3s(^1P_1)nd$ and $2p^5 3s(^1P_1)ns$ autoionizing resonances observed in the photoabsorption spectrum of sodium in the $2p$-subshell excitation region show remarkable similarity to that of the autoionizing resonances $mp^5(^2P_{1/2})nd[3/2]_1$ and $ns[3/2]_1$ in inert gases. The observed overlapping series of autoionizing resonances have been parametrized using a three-channel quantum-defect-theory approach, one open and two bound channels. A simple n-channel MQDT relation in terms of cofactors is presented to calculate the photoionization cross section for one open and $(n-1)$ bound channels. As the generalized expression is derived in terms of cofactors, the computer code for a higher number of interacting channels remains practically the same and runs almost as fast as for the two or three interacting channels model.

] U. Fano, Phys. Rev. **124**, 1866 (1961).
] J. P. Connerade *et al.*, Astro. Phys. J. **165**, 203 (1971).
] H. Wolff *et al.*, Z. Phys. **252**, 353 (1972).
] W. E. Cooke and C. L. Cromer, Phys. Rev. A **32**, 2725 (1984).
] A. Giusti-Suzor and U. Fano, J. Phys. B **17**, 215 (1984).
] A. Giusti-Suzor and H. Lefebvre-Brion, Phys. Rev. A **30**, 3057 (1984).
] K. Ueda, Phys. Rev. A **35**, 2484 (1987).
] H. Hieronymus *et al.*, J. Phys. B **25**, 3463 (1992).
] M. A. Baig *et al.*, J. Phys. B **17**, L271 (1984).
] M. A. Baig and J. P. Connerade, J. Phys. B **17**, 1785 (1984).
[11] M. A. Biag, J. P. Connerade, and M. Pantelorous (unpublished).
[12] K. Yoshino, J. Opt. Soc. Am. **60**, 536 (1970).
[13] K. Yoshino and Y. Tanaka, J. Opt. Soc. Am. **69**, 159 (1979).
[14] R. D. Bonin *et al.*, J. Opt. Soc. Am. B **2**, 1275 (1985).
[15] K. Ito *et al.*, J. Opt. Soc. Am. B **5**, 2006 (1988).
[16] K. T. Lu and U. Fano, Phys. Rev. A **2**, 81 (1970).
[17] C. J. Dai *et al.*, J. Opt. Soc. Am. B **6**, 1486 (1989).
[18] G. Racah, Phys. Rev. **61**, 546 (1942).
[19] R. D. Cowan, *The Theory of Atomic Structure and Spectra* (University of California Press, Berkeley, 1981).